Investigating the Role of Symptom Severity on Health Economic Outcomes

Phoebe Asplin[a]

[a]*Mathematics for Real-World Systems Centre for Doctoral Training, University of Warwick, Coventry, CV4 7HP, United Kingdom*

ARTICLE INFO

Keywords:
respiratory pathogens
symptom severity
cost-effectiveness

ABSTRACT

Respiratory infections pose a serious risk to public health, which comes with a considerable economic cost. This makes them a significant focus for epidemiological and health economic research.

In traditional models of infectious diseases, the symptom severity of an infected individual does not impact the symptom severity of those infected by them. However, there is evidence in the literature that an individual's disease severity may pass on to those they infect, creating a mapping between the symptom severity of the infector and infectee.

This report establishes the importance of a symptom severity mapping on epidemiological and health economic outcomes. Here I demonstrate that a symptom severity mapping led to a larger proportion of cases being severe compared to the scenario with no such mapping. Furthermore, a partial symptom severity mapping led to a reduction in total infections when compared to the expected final size, even when R_0 was fixed. When modelling an intervention with a symptom-blocking effect, I found that the inclusion of a symptom severity mapping led to the intervention preventing more infections and hospitalisations, making it more cost-effective. Additionally, the strength of the symptom severity mapping determined the optimal intervention uptake when the efficacy of the intervention was high.

These results demonstrate the importance of a symptom severity mapping, suggesting a need for further research into the transmission mechanisms of respiratory pathogens to determine if and how symptoms pass on with infection. This report also motivates further research to continue to establish the importance of a symptom severity mapping on questions relevant to public health policy.

1. Introduction

Respiratory pathogens are those that cause infections in the respiratory tract. These pathogens mainly cause mild disease with symptoms focused in the upper respiratory tract. However, such pathogens have the potential to infect lower into the respiratory tract, causing severe symptoms. Lower respiratory tract infections account for more than 2.4 million deaths worldwide each year (Lozano et al., 2012) and are a leading cause of global mortality, especially amongst children and the elderly (Wardlaw et al., 2006). These pathogens tend to be highly transmissible, with their tendency to mild disease often helping them spread through a population undetected (Forum of International Respiratory Societies, 2021).

For example, in 2019, *SARS-CoV-2*, the causative agent of COVID-19 disease, became a respiratory pathogen of international concern. Its highly transmissible nature led to its spread across the globe and subsequent declaration as a pandemic in 2020 (UK Health Security Agency, 2022). *SARS-CoV-2* also carries a high risk of causing severe COVID-19 disease amongst the elderly and those with underlying medical issues, resulting in an estimated 5.5 million global deaths by the end of 2021 (World Health Organisation, 2022a). Here the World Health Organisation (2022b) define a COVID-19 death as one caused by a "clinically compatible illness, in a probable or confirmed COVID-19 case, unless there is a clear alternative cause of death". In addition, COVID-19 massively impacted the global economy, with the global cost in 2020 and 2021 estimated to be 14% of 2019 GDP (González López-Valcárcel and Vallejo-Torres, 2020). This was partially due to the high cost of interventions. As of September 2021, the UK had spent £17.9bn on

the test and trace programme, £13.8bn on the procurement of personal protective equipment and £1.8bn on vaccine and antibody supply (Appleby, 2022).

Many respiratory diseases have pandemic potential, including other coronaviruses, such as SARS (National Health Service, 2019), and pandemic strains of influenza which have historically had devastating effects. For example, the 1918/19 Spanish flu pandemic is thought to have resulted in 50 million deaths worldwide (Centers for Disease Control and Prevention, 2019), and the 2009 H1N1 pandemic caused 200,000 deaths in its first year of circulation (Dawood et al., 2012). Additionally, seasonal influenza causes annual epidemics which, prior to the COVID-19 pandemic, were estimated to result in symptomatic infection of 8% of the US population each year on average (Tokars et al., 2018) and around 290,000 to 650,000 deaths globally (World Health Organisation, 2018). These epidemics affect people of all ages, but the elderly and those with co-morbidities tend to face the most severe disease and highest mortality rates (Cromer et al., 2014).

Respiratory diseases pose a serious risk to public health, which comes with a considerable economic cost. This makes them a significant focus for epidemiological research and motivates the use of optimal intervention strategies. Research into the cost-effectiveness of an intervention has to consider not only the cost of the intervention but also the epidemiological outcomes. The threat of respiratory diseases also motivates research into their transmission mechanisms, including the relationship between viral load and severity of illness and the routes of transmission through which they spread.

In models of infectious diseases, the symptom severity of an infected individual does not usually impact the symptom severity of those infected by them. However, the literature suggests that an individual's disease severity may pass on to those they infect. This means that infection by an individual with severe disease would be more likely to be severe than if the infecting individual had mild disease. Therefore a mapping between the symptom severity of the infector and infectee is formed.

There are two pathways through which symptom severity is hypothesised to be passed on with infection. The first pathway is through a dose-response relationship. Severe disease is correlated with higher viral shedding (Couch et al., 1971; Chu et al., 2004; Al-Abdely et al., 2019) meaning those infected will receive a larger infectious dose which in turn leads to more severe disease (Aaby and Coovadia, 1985; Jones and Su, 2015). The second pathway is through differential transmission routes. It is hypothesised that severe disease is primarily transmitted through aerosol transmission (transmission involving particles smaller than $5\mu m$ which are sufficiently small and light to travel on air flows) as opposed to close contact transmission (transmission involving direct or indirect contact with an infected individual or transmission via large droplets) (Killingley and Nguyen-Van-Tam, 2013). Infection via aerosol transmission is then in turn likely to cause more severe disease (Tellier, 2009; Gani and Leach, 2004; Tellier, 2022). I explored the evidence supporting the existence of the pathways and included a summary of the literature for plague, influenza and COVID-19 in Supplementary Information S1.

A potential symptom severity mapping has not been explored in depth within mathematical modelling studies of respiratory diseases, but studies have considered the factors that might contribute to this effect.

First, it has become common for models to include asymptomatic infections with reduced or no transmission, motivated by asymptomatic transmission being thought to contribute significantly to the spread of *SARS-CoV-2* (Moghadas et al., 2020). Asymptomatic infections are generally assumed to occur with a fixed probability, independent of other infected individuals (Mathews et al., 2007). However, Harris et al. (2022) investigated the impact of asymptomatic transmission of SARS-CoV-2 on the resulting disease severity. The authors considered the effect of disease status (i.e. asymptomatic or symptomatic disease) on transmission outcomes. They found that when infectious periods of asymptomatic and symptomatic infections were equal, the correlation between disease status

and transmission outcomes did not affect the outbreak dynamics. Yet, if the infectious period differed, this correlation exaggerated the effect of the difference. Beyond these results, the exploration of a symptom severity mapping was limited.

Second, Paulo et al. (2010) hypothesised that disease severity of influenza was dependent on infectious dose, motivated by the increase in case-fatality ratio (CFR) in army camps compared to civilian communities during the 1918 influenza pandemic. Such a dose-response relationship was applied to a susceptible-exposed-infectious-recovered (SEIR) transmission model and was found to result in the observed difference in CFR. Within this model, the infectious dose depended on the number of infected individuals but not their disease severity.

Finally, many mathematical modelling studies have considered multi-route transmission models - particularly for influenza (Atkinson and Wein, 2008; Smieszek et al., 2019). These studies aimed to establish the relative importance of different transmission routes and subsequently the effectiveness of interventions targeting specific routes. However, these studies did not consider the impact of transmission routes on symptom severity or vice versa. These mechanisms have started to be investigated regarding *SARS-CoV-2*, which is thought to spread through both aerosol and close contact transmission (Tellier, 2022; Andersson, 2021). Wu et al. (2020)'s pre-print evaluated the impact of transmission routes on COVID-19 disease severity, arguing that interventions targeting aerosol transmission should be prioritised to limit the spread of severe disease.

Whilst the studies mentioned have begun to at least partially investigate a potential symptom severity mapping, none have considered the impact of symptom severity mappings on health economic outcomes. Previous health economic studies have focused on the cost-effectiveness of vaccination scenarios, especially within the context of seasonal influenza (Hill et al., 2020; Thorrington et al., 2019). Many health economic modelling studies of COVID-19 have similarly focused on vaccine rollout (Kohli et al., 2021). However, some have focused on symptom-dependent interventions, such as comparing the effectiveness of symptomatic vs asymptomatic testing (Neilan et al., 2021) and considering quarantining measures that predominantly target symptomatic individuals (Zala et al., 2020).

This report added to the research by using a compartmental ODE model to analytically and computationally explore the effect of a symptom severity mapping on epidemiological outcomes in addition to exploring the sensitivity of the system to infectious period and transmissibility of severe disease. I also investigated the effect of a symptom severity mapping on health economic outcomes by exploring the cost-effectiveness of an intervention with a symptom-reducing effect.

I found that the dependence of symptoms on the infector's symptom severity substantially affects the value of R_0 through an analytical exploration of the model. When exploring the model computationally for fixed values of R_0, the dependence on infector severity led to large changes in the proportion of cases that are severe and the total number of infections. When introducing an intervention with a symptom-reducing effect, the dependence on symptom severity notably impacted the cost-effectiveness and optimal uptake of the intervention. These findings suggest that research into a symptom severity mapping is imperative to finding the optimal intervention strategy for a specific respiratory disease.

2. Methods

To investigate the spread of a respiratory pathogen throughout the UK, I used a compartmental ODE model based on the standard SEIR framework. Initially, the model was developed to apply to any number of symptom severity levels (Section 2.1). However, to enable gathering broad insights, the model used in most of the analysis had two symptom severity levels (Section 2.2).

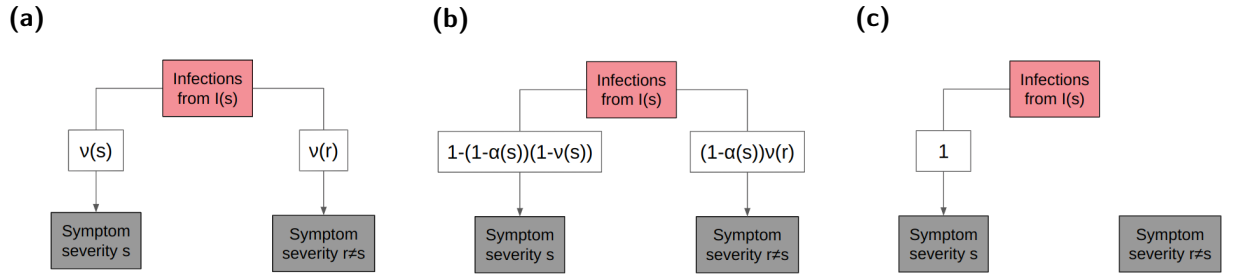

Figure 1: The proportion of cases with each symptom severity level resulting from infections by individuals with symptom severity s. I present three cases dependent on the value of α: (a) $\alpha = 0$; (b) $\alpha \in [0, 1]$; (c) $\alpha = 1$. Here $\nu(s)$ is the baseline probability of having symptom severity s and $\alpha(s)$ is the dependence on the infector's symptom severity when the infector has symptom severity s.

Within this section, I have presented the ODE model used throughout the analysis which accounts for a symptom severity mapping. After this is described for n symptom severity levels, I described the model and parameters used for two symptom severity levels: mild and severe. Next, I described the intervention used and the updated ODE model before explaining how the health economic outputs relating to the intervention were calculated and the parameters during that analysis.

2.1. SEIR model for n symptom severity levels

I began by considering a generalised version of the model with n symptom severity levels. All classes except for the susceptible class were separated into n compartments representing different symptom severity levels $s \in \hat{S}$. $E(s)$ contains individuals exposed to the disease who will develop disease with symptom severity s. $I(s)$ contains individuals who have become infectious and are now exhibiting symptom severity s. I assumed there was no movement between the severity classes, meaning an individual's severity would be constant across their infectious period.

Description of the transmission dynamics

The transmission rates, $\beta(s)$, and recovery rates, $\gamma(s)$, depended on the disease severity. The incubation period, and thus the rate of becoming infectious, ϵ, was constant across all severity levels. I assumed that transmission was frequency-dependent - meaning that the force of infection increases with the proportion of the population infected but not the overall population size - as this is a typical assumption used when modelling human respiratory diseases. Additionally, I assumed there is no waning immunity after recovery and no demography (natural births and deaths) since the outbreaks were assumed to occur over a short time frame where the impacts of these processes would be negligible.

Description of the symptom severity mapping

To include a symptom severity mapping into the model, I defined the parameter $\alpha(s)$ to be the dependence on the symptom severity of the infector when the infector has symptom severity s. When $\alpha(s) = 0$, there is no dependence on the infector's symptom severity and the symptom severity of the infected individual depends entirely on ν (Fig. 1(a)). $\nu(s)$ is the baseline probability of having symptom severity level s. For $\alpha(s) \in [0, 1]$, there is a partial dependence on the infector's symptom severity and a partial dependence on $\nu(s)$ (Fig. 1(b)). When $\alpha(s) = 1$, the symptom severity of an infected individual is wholly dependent on that of their infector, meaning that symptom severity is always passed on with infection (Fig. 1(c)).

The equations below show the model at the edge cases.

If $\alpha(s) = 0$ for all $s \in \mathcal{S}$:

$$\begin{aligned}
\frac{dS}{dt} &= -\sum_{s\in\hat{\mathcal{S}}} \lambda(s)S \\
\frac{dE(s)}{dt} &= \nu(s)\sum_{r\in\hat{\mathcal{S}}} \lambda(r)S - \epsilon E(s) \\
\frac{dI(s)}{dt} &= \epsilon E(s) - \gamma(s)I(s) \\
\frac{dR(s)}{dt} &= \gamma(s)I(s)
\end{aligned}$$

If $\alpha(s) = 1$ for all $s \in \mathcal{S}$:

$$\begin{aligned}
\frac{dS}{dt} &= -\sum_{s\in\hat{\mathcal{S}}} \lambda(s)S \\
\frac{dE(s)}{dt} &= \lambda(s)S - \epsilon E(s) \\
\frac{dI(s)}{dt} &= \epsilon E(s) - \gamma(s)I(s) \\
\frac{dR(s)}{dt} &= \gamma(s)I(s)
\end{aligned}$$

These equations are then generalised to all values of α in Eq. (1). The proportion of the S class moving into $E(s)$ is given by

$$\Big(1 - \big(1-\alpha(s)\big)\big(1-\nu(s)\big)\Big)\lambda(s) + \sum_{r\in\hat{\mathcal{S}}/\{s\}} \big(1-\alpha(r)\big)\nu(s)\lambda(r)$$

Here the first term contains those who are the same severity as their infector and the second contains those who are infected by individuals with a different symptom severity level. The latter can be considered as developing symptom severity s randomly due to the background probability of having any severity level.

$$\begin{aligned}
\frac{dS}{dt} &= -\sum_{s\in\hat{\mathcal{S}}} \lambda(s)S \\
\frac{dE(s)}{dt} &= \left(\Big(1 - \big(1-\alpha(s)\big)\big(1-\nu(s)\big)\Big)\lambda(s) + \sum_{r\in\hat{\mathcal{S}}/\{s\}} \big(1-\alpha(r)\big)\nu(s)\lambda(r)\right)S - \epsilon E(s) \\
\frac{dI(s)}{dt} &= \epsilon E(s) - \gamma(s)I(s) \\
\frac{dR(s)}{dt} &= \gamma(s)I(s)
\end{aligned} \tag{1}$$

where $\lambda(s)$ is the force of infection from those with symptom severity s, given by:

$$\lambda(s) = \frac{\beta(s)I(s)}{N}$$

Calculating R_0

The basic reproductive number, R_0, is commonly used in epidemiology to indicate a disease's potential to spread through a population. It is defined as the average number of secondary cases generated by an average infectious individual in a fully susceptible population. R_0 can then be written as

$$R_0 = \text{(average number of infections generated per unit time)} \times \text{(average infectious period)}$$

I calculated the value of R_0 using the next-generation matrix (NGM) approach. This method was developed by Diekmann et al. (1990) to calculate the value of R_0 in heterogeneous populations where compartments are split into a

finer structure (e.g. into age classes). The next generation matrix is defined to be

$$\mathbf{K} = \begin{pmatrix} k_{11} & \cdots & k_{1n} \\ \vdots & & \vdots \\ k_{n1} & \cdots & k_{nn} \end{pmatrix}$$

where k_{ij} is the average number of type-i cases generated by a type-j case in a fully susceptible population. I applied this to the ODE model by considering a vector containing the number of people in each infectious class, which then multiplies by $\mathbf{K}$ at each time step. This vector grows at a rate given by the dominant eigenvalue of $\mathbf{K}$ - the eigenvalue with the largest absolute value. Therefore, R_0 is this dominant eigenvalue. Using this method, I analytically explored the impact of a symptom severity mapping on the value of R_0 (Section 3.1).

2.2. SEIR model for two symptom severity levels

To aid parameterisation of the model, and in keeping with the granularity of data presently available, I simplified the system to have two symptom severity levels. Whilst this model applies to a range of respiratory diseases, I used influenza throughout the analysis to demonstrate the usefulness of the framework.

Description of the two symptom severity levels

No formal scheme exists for distinguishing between different severity levels of influenza infection. Some papers refer to "mild" or "severe" cases whilst others refer to "asymptomatic" or "symptomatic" cases. In this report, I use the terms "mild" and "severe" to distinguish disease severity. Severe disease is generally associated with the development of a cough and fever (Mathews et al., 2007; Little et al., 1979; Cowling et al., 2013). I have associated severe disease with the development of a cough since it is amenable to being measured and thus recorded in the majority of experimental studies.

Description of the transmission dynamics

The model for two symptom severity levels was governed by the following system of equations:

$$\begin{aligned}
\frac{dS}{dt} &= -\frac{\beta_M S I_M}{N} - \frac{\beta_S S I_S}{N} \\
\frac{dE_M}{dt} &= (1-(1-\alpha_M)\nu)\frac{\beta_M S I_M}{N} + (1-\alpha_S)(1-\nu)\frac{\beta_S S I_S}{N} - \epsilon E_M \\
\frac{dE_S}{dt} &= (1-\alpha_M)\nu\frac{\beta_M S I_M}{N} + (1-(1-\alpha_S)(1-\nu))\frac{\beta_S S I_S}{N} - \epsilon E_S \\
\frac{dI_M}{dt} &= \epsilon E_M - \gamma_M I_M \\
\frac{dI_S}{dt} &= \epsilon E_S - \gamma_S I_S \\
\frac{dR_M}{dt} &= \gamma_M I_M \\
\frac{dR_S}{dt} &= \gamma_S I_S
\end{aligned} \tag{2}$$

Here the notation E_M and E_S denote those who have been exposed to the disease and will go on to develop mild or severe disease respectively, I_M and I_S denotes those who are infectious are and exhibiting mild or severe disease, and R_M and R_S contain individuals who have recovered from mild or severe disease.

Table 1
Description of parameters used in the SEIR model based on data for influenza.

Parameter	Description	Value	Source
β_M	Mild transmission rate	β	
β_S	Severe transmission rate	2β	
ν	Probability of symptoms being severe	0.2	Carrat et al. (2008)
ϵ	Rate of becoming infectious	0.5	Carrat et al. (2008); Cowling et al. (2013)
γ_M	Mild recovery rate	1/5	Carrat et al. (2008); Cao et al. (2009)
γ_S	Severe recovery rate	1/7	Carrat et al. (2008); Cao et al. (2009)

The parameters for this model (Table 1) are based on data for influenza. In this model, $\nu_S = \nu$ and $\nu_M = 1 - \nu$ and severe disease were assumed to be twice as transmissible as mild disease.

The value of β was chosen to fix a value of R_0. This was done by deriving an equation for R_0, using the NGM approach (see Section 3.2). Note that R_0 was fixed without also fixing r as this varies for different values of γ_S. I chose the fixed values of R_0 to reflect a range of disease scenarios. $R_0 = 1.1$ describes a disease that will spread through a population slowly and requires minimal interventions to die out. $R_0 = 2.0$ represents a seasonal epidemic such as seasonal influenza. $R_0 = 3.0$ represents a highly transmissible pathogen with pandemic potential, such as *SARS-CoV-2* or pandemic influenza.

Using these equations, I explored the model analytically by investigating the effect of α_M and α_S on the value of R_0 (see Section 3.1). I then explored the model's sensitivity to $\alpha = \alpha_M = \alpha_S$. I investigated how α affected the proportion of cases that were severe, the proportion of the population infected at the outbreak's peak and the final size of the outbreak (see Section 3.3). The final size was compared to that expected from an SEIR model no heterogeneity in symptom severity (see Supplementary Information S2).

2.3. Modelling a symptom-blocking intervention

To investigate the impact of a symptom severity mapping on the effectiveness of an intervention, I considered an intervention with a symptom-reducing effect.

Description of the intervention

I assumed the intervention was one used during the infectious period to reduce the presentation of symptoms, so it did not have a susceptibility-reducing effect. Those with access to the intervention were assumed to have the same probability of having a certain symptom severity level, but if they have severe disease, they had a set probability (given by the efficacy, η) of the intervention reducing their onwards transmission to that of mild infections. This meant that their transmission rate was reduced to the mild transmission rate, and they were assumed to have mild disease when considering the symptom severity of those they infect. However, their infectious period remained the length of the severe infectious period as the intervention only affects their onwards transmission. I assumed the intervention was leaky, meaning it was not 100% effective.

At the start of each simulation, it was assumed that a set proportion of the population (given by the uptake, u) would be given access to the intervention. They would then use the intervention if they were infected. I assumed no additional individuals were given access to the intervention throughout the simulation.

Description of the model equations

Since those using the intervention and those not using the intervention are equally likely to move into a particular symptom severity class and have the same parameters, the equations governing the system for both groups are the same. Thus the intervention only changed the force of infection terms which became

$$\lambda_M = \frac{\beta_M(I_M + \eta u I_S)}{N}$$

$$\lambda_S = \frac{\beta_S(1-\eta u)I_S}{N}$$

Therefore, the model only depends on the value of ηu. It was possible to simplify the equations to use a single parameter equal to ηu. However, as I aimed to explore the per unit cost at which the intervention became cost-effective, it was important that I could distinguish between the uptake and the efficacy of the intervention.

The intervention was then run for a range of values of α and ν (both between 0 and 1 with an increment of 0.02), for each of which β was chosen to fix $R_0 = 3.0$ in the no intervention case. Then, within each of these scenarios, I explored the model's sensitivity to the intervention's uptake and efficacy. This analysis consisted of an exploration of the intervention's impact on the total number of infections, the number of severe infections and the number of hospitalisations (see Section 3.4). The number of hospitalised cases is calculated from the total number of infections at the end of the simulation. It is assumed that 1% of severe cases result in hospitalisation and mild cases never result in hospitalisation. Those with severe disease using the intervention are considered to present with mild symptoms with probability η. Those cases are also assumed to never result in hospitalisation.

In addition to this intervention, I constructed an ODE model for an intervention that has a susceptibility-reducing effect and reduces the presentation of symptoms (see Supplementary Material S3). The analysis of this model is a direction for further study.

2.4. Health economic modelling

Often there are many potential intervention strategies that can be used to limit the spread of the disease. Since governing bodies have a limited budget to spend on public health, the cost of the intervention is an important factor to consider alongside the resulting epidemiological outcomes. Thus, measures for both the benefit to public health and the costs associated with the intervention and treatment, are required.

Quality-adjusted life years (QALYs) are a measure of disease burden that consider both the quality and quantity of years lived. One QALY is equivalent to one year in perfect health. The QALY score ranges depending on the severity of the disease, with 0 being equivalent to death and 1 being perfect health. The willingness to pay (WTP) threshold per QALY is the amount a governing body is willing to pay to gain one QALY.

Calculating QALY losses

The QALY losses for each disease severity are shown in Table 2. I assumed that mild disease had sufficiently minimal symptoms to cause no QALY losses. The QALY losses per death depend primarily on the number of healthy years lost and therefore the age of the individual. My model was not stratified by age class, so to estimate the average QALY losses per death, I used data from an outbreak in Spain during the 2009 H1N1 pandemic Hollmann et al. (2013) and divided the total QALY loss from deaths by the number of deaths.

The number of hospitalised cases was as described in the previous section, giving that

$$\text{Total hospitalisations} = 0.01\big((1-\eta u)R_S(\infty)\big)$$

Table 2
Description of parameters used in the health economic modelling.

Description	Value	Source
Hospitalisation rate of severe disease	0.01	Hill et al. (2020)
Death rate of severe disease	0.001	Hill et al. (2020)
QALY loss from a mild case	0 QALYs	Hill et al. (2020)
QALY loss from a severe, non-hospitalised case	0.008 QALYs	Hill et al. (2020)
QALY loss from a non-fatal hospitalised case	0.018 QALYs	Hill et al. (2020)
QALY loss from a fatal hospitalised case	37.5 QALYs	Hollmann et al. (2013)
Total cost of a non-fatal hospitalised case	£1,300	Hill et al. (2020)
Total cost of a fatal hospitalised case	£2,600	Hill et al. (2020)
Willingness to pay threshold per QALY	£20,000	Hill et al. (2020)

where $R_S(\infty)$ is the number of individuals in the R_S class at the end of the simulation or, equivalently, the total number of severe infections.

The number of cases resulting in deaths was calculated similarly to the hospitalisations, with 0.1% of severe cases resulting in death. These deaths were assumed to be a subset of hospitalisations, meaning that all deaths resulted from a hospitalised case. The total number of deaths was given by

$$\text{Total deaths} = 0.001\big((1-\eta u)R_S(\infty)\big)$$

Usually, discounting is used in health economic modelling. This is where a lower value is assigned to costs and health outcomes that occur in the future (Smith et al., 2001). In all scenarios, the outbreak lasts less than a year, so no discounting was required for QALY losses occurring in later years.

The number of severe cases, hospitalisations and deaths are then compared to those from the no intervention scenario to give the prevented number of severe cases, hospitalisations and deaths. From this, I calculated the QALYs gained by the intervention.

Calculating the cost of the intervention

In addition to QALYs lost, hospitalised cases have an associated cost as described in Table 2. An effective intervention reduces the number of hospitalisations, preventing the related costs. The prevented costs are taken away from the overall cost of the intervention:

$$\text{Overall cost} = (\text{intervention cost per unit}) \times (\text{uptake}) \times N - (\text{hospital costs prevented})$$

Calculating the threshold intervention cost

The intervention was deemed to be cost-effective if the overall cost was less than or equal to the willingness to pay (the product of the Threshold WTP per QALY and QALYs gained). Equivalently,

$$(\text{Per unit intervention cost}) \leq \frac{(\text{WTP threshold}) \times (\text{QALY loss prevented}) + (\text{hospital costs prevented})}{\text{uptake} \times N}$$

From this I calculated the threshold per unit intervention cost for an intervention scenario.

For set values of α (0, 0.2, 0.5, 0.8, 1), ν (0.2, 0.5, 0.8) and η (25%, 50%, 70%, 90%), I then found the optimal intervention uptake by maximising the threshold per unit intervention cost. When this was maximised, the intervention was most cost-effective.

2.5. Simulation overview

Using the models described in the previous sections, I simulated an outbreak within a population the size of the UK ($N = 67$ million). All the scenarios begin with one infectious individual in each of the symptom severity classes (I_M and I_S) and the remainder of the population were initially susceptible (in the S class). The simulations were run until there was less than one individual in all the infected classes (E_M, E_S, I_M and I_S). These simulations were performed using Matlab R2022a.

3. Results

Initially, I explored the value of R_0 analytically to investigate how it changed with the dependence on the infector's symptom severity, α.

3.1. Calculating R_0 for the n-level symptom severity model

Let $\hat{S} = \{s_1, \dots, s_n\}$ be the set of symptom severity levels. Applying the NGM method to the set of ODEs for n symptom severity levels (Eq. (1)), the average number of type-i cases generated in a fully susceptible population by a type-i case, k_{ii}, is:

$$k_{ii} = \Big(1 - \big(1 - \alpha(s_i)\big)\big(1 - \nu(s_i)\big)\Big)\frac{\beta(s_i)}{\gamma(s_i)}$$

and by a type-j case, k_{ij}, is

$$k_{ij} = \big(1 - \alpha(s_j)\big)\nu(s_i)\frac{\beta(s_j)}{\gamma(s_j)}$$

.

When $\alpha(s_i) = 0$ for all $i \in \{1, \dots, n\}$, $\mathbf{K}$ becomes the product of two vectors

$$\mathbf{K} = \left(\frac{\beta(s_1)}{\gamma(s_1)}, \cdots, \frac{\beta(s_n)}{\gamma(s_n)}\right)^T \Big(\nu(s_1), \cdots, \nu(s_n)\Big)$$

Any matrix in $\mathbb{R}^{n\times n}$ of the form $A = u^T v$ has $n - 1$ zero eigenvalues and an eigenvalue $\lambda = \text{Trace}(u^T v)$ (Dattorro, 2006). So the dominant eigenvalue is

$$\begin{aligned} R_0 &= \sum_i k_{ii} \\ &= \sum_i \nu(s_i)\frac{\beta(s_i)}{\gamma(s_i)} \end{aligned}$$

When $\alpha(s_i) = 1$ for all $i \in \{1, \dots, n\}$, $\mathbf{K}$ becomes

$$\mathbf{K} = \begin{pmatrix} \frac{\beta(s_1)}{\gamma(s_1)} & 0 & \cdots & 0 \\ 0 & \frac{\beta(s_2)}{\gamma(s_2)} & \cdots & 0 \\ \vdots & \vdots & \ddots & \vdots \\ 0 & 0 & \cdots & \frac{\beta(s_n)}{\gamma(s_n)} \end{pmatrix}$$

As **K** is a diagonal matrix, its eigenvalues are its diagonal entries so the dominant eigenvalue is

$$R_0 = \max_i \left(\frac{\beta(s_i)}{\gamma(s_i)} \right)$$

When extending this to explore R_0 for general values of α, I found that the possible analytical insight was limited for the n-level model. In order to further explore the system, I used the two severity ODE model described in Section 2.2.

3.2. Calculating R_0 for the two-level symptom severity model

I then considered two symptom severity levels, mild and severe. In this case,

$$\mathbf{K} = \begin{pmatrix} k_{MM} & k_{MS} \\ k_{SM} & k_{SS} \end{pmatrix} = \begin{pmatrix} \frac{\beta_M}{\gamma_M}(1-(1-\alpha_M)\nu) & \frac{\beta_S}{\gamma_S}(1-\alpha_S)(1-\nu) \\ \frac{\beta_M}{\gamma_M}(1-\alpha_M)\nu & \frac{\beta_S}{\gamma_S}(1-(1-\alpha_S)(1-\nu)) \end{pmatrix}$$

Calculating R_0 when $\alpha_M = \alpha_S$

Initially, I set $\alpha_S = \alpha_M = \alpha$, to explore the system at the extreme values of α. As in the n dimension case, if $\alpha = 0$, meaning symptoms are independent of their infector's, then

$$R_0 = \nu \frac{\beta_S}{\gamma_S} + (1-\nu)\frac{\beta_M}{\gamma_M}$$

In effect, the value of R_0 was the average of the R_0 values for the mild and severe groups.

If $\alpha = 1$, meaning that symptoms always pass on with infections, then

$$R_0 = \max\left(\frac{\beta_S}{\gamma_S}, \frac{\beta_M}{\gamma_M} \right)$$

So R_0 is entirely governed by the symptom severity which creates the most secondary infections.

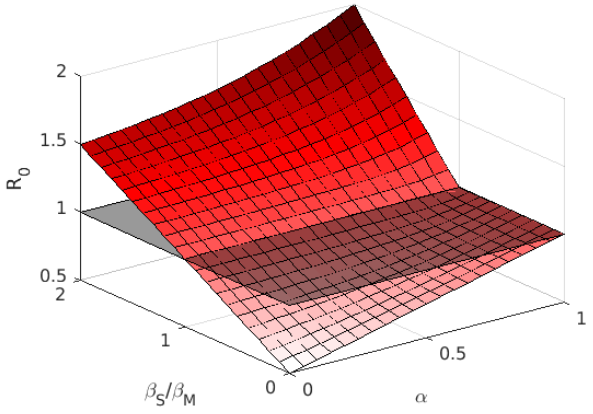

Figure 2: Investigating the value of R_0 whilst varying the dependence on the infector's symptom severity and the ratio of the transmission rates. Here $\beta_M = 0.2$ and β_S was varied to give the required ratio. Severe and mild disease have an equal probability of occurring ($\nu = 0.5$) and equal infectious periods $\gamma_S = \gamma_M = 1/5$. R_0 was calculated using Eq. (5) (see Supplementary Information S4) and the grey plane corresponds to $R_0 = 1$.

I then explored the effect of changing the ratio of the transmission rates, β_S/β_M, on R_0 by fixing β_M and varying β_S. Assuming that severe and mild disease have an equal probability of occurring ($\nu = 0.5$) and equal infectious periods $\gamma_S = \gamma_M = \gamma$, I found that the value of α affected the qualitative relationship between β_S/β_M and R_0 (Fig. 2). When $\alpha = 0$, R_0 increased linearly with $\frac{\beta_S}{\beta_M}$ with $R_0 = \frac{1}{2\gamma}(\beta_M + \beta_S)$. When $\alpha = 1$, $R_0 = \frac{1}{\gamma}\max(\beta_M, \beta_S)$. So, when $\beta_S/\beta_M > 1$, R_0 increased linearly and when $\beta_S/\beta_M < 1$ R_0 remained constant at $\frac{\beta_M}{\gamma}$.

Calculating R_0 when $\alpha_M \neq \alpha_S$

Next, considering when α_S and α_M had distinct values (Fig. 3), I found that when $\alpha_S = 1$ or $\alpha_M = 1$, one of the off-diagonal elements of $\mathbf{K}$ would be equal to zero and therefore the eigenvalues were again given by the diagonal elements. So

$$R_0 = \max\left(\frac{\beta_M}{\gamma_M}\big(1-(1-\alpha_M)\nu\big), \frac{\beta_S}{\gamma_S}\big(1-(1-\alpha_S)(1-\nu)\big)\right)$$

If $\alpha_S = 1$ this becomes

$$R_0 = \max\left(\frac{\beta_M}{\gamma_M}\big(1-(1-\alpha_M)\nu\big), \frac{\beta_S}{\gamma_S}\right)$$

and if $\alpha_M = 1$ this becomes

$$R_0 = \max\left(\frac{\beta_M}{\gamma_M}, \frac{\beta_S}{\gamma_S}\big(1-(1-\alpha_S)(1-\nu)\big)\right)$$

In this scenario, severe disease was assumed to be more transmissible and has a longer infectious period than mild disease, meaning that $\frac{\beta_S}{\gamma_S} > \frac{\beta_M}{\gamma_M}$. This led to α_S having a larger impact on R_0 than α_M. R_0 attained a maximum when $\alpha_S = 1$ and a minimum when $\alpha_M = 1$ and $\alpha_S \in [0, 0.2]$ for this set of parameters (Fig. 3).

When $\alpha_S = 1$, R_0 remained constant with $R_0 = \frac{\beta_S}{\gamma_S}$ as α_M varies, since $\frac{\beta_S}{\gamma_S} > \frac{\beta_M}{\gamma_M}(1-\nu)$. On the other hand, when $\alpha_M = 1$, $R_0 = \frac{\beta_S}{\gamma_S}(1-(1-\alpha_S)(1-\nu))$ until the value of α_S which satisfied $\frac{\beta_S}{\gamma_S}(1-(1-\alpha_S)(1-\nu)) = \frac{\beta_M}{\gamma_M}$. For lower values of α_S the value of R_0 switched to become $\frac{\beta_M}{\gamma_M}$.

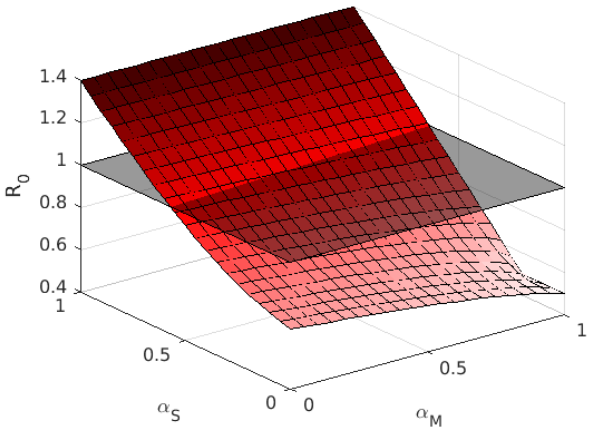

Figure 3: Investigating the value of R_0 whilst varying the dependence on infector's symptom severity when they have mild or severe disease (α_M and α_S respectively). Here the parameters are as given in Table 1 ($\nu = 0.2$, $\gamma_M = 1/5$ and $\gamma_S = 1/7$) and the transmission rates are set to be $\beta_M = 0.1$ and $\beta_S = 0.2$. R_0 is calculated using Eq. (5) (see Supplementary Information S4) and the grey plane is where $R_0 = 1$.

Varying parameters for fixed values of R_0

Since the eigenvalues of **K** can be computed, it is possible to derive an equation for R_0 that can be solved for a given parameter set (see Supporting Information S4).

If $\beta_M = \beta$, $\beta_S = r\beta$, R_0 is fixed and $\alpha_M = \alpha_S = \alpha$, then the derived equation for R_0 (Eq. (4) in Supporting Information S4) simplifies to

$$\frac{r(1-\alpha)}{\gamma_M\gamma_S}\beta^2 - R_0\left(\frac{(1-\alpha\nu)}{\gamma_M} + \frac{r(1-\alpha(1-\nu))}{\gamma_S}\right)\beta - R_0^2 = 0 \tag{3}$$

Using this equation, I investigated varying α whilst keeping R_0 and r fixed by choosing a suitable value of β or similarly investigate the effect of changing r for a fixed value of R_0 and α.

3.3. Sensitivity analysis

To expand on the results from the previous section, I explored the two symptom severity model computationally. Having established that α had a substantial effect on the value of R_0, I fixed R_0 for each set of runs in this analysis. This allowed me to explore the impact of varying α on other epidemiological outputs. I fixed the value of R_0 by choosing an appropriate value of β for each value of α, using Eq. (3).

Unless stated otherwise, the parameters used in this section are as given in Table 1. I assumed throughout that $\alpha_M = \alpha_S = \alpha$ and initially assumed $\frac{\beta_S}{\beta_M} = 2$, where $\beta_M = \beta$ and $\beta_S = 2\beta$. Note that, at points during this analysis, γ_S and β_S/β_M were varied alongside α.

Epidemiological outputs are highly sensitive to α

I began by investigating the effect of the dependence on the infector's symptom severity, α, on the proportion of the population infected across the whole simulation (Fig. 4(a)) and at the peak of the outbreak (Fig. 4(b)). I did so for three values of R_0: 1.1, 2.0 and 3.0.

I found that for all three values of R_0, the effect of α was consistent, although the total number of cases and peak number of cases were higher for larger values of R_0 as expected. The total proportion of the population infected was similar across values of α, but the proportion of those cases that were severe varied dramatically. When $\alpha = 1$, (symptoms always pass on with infection) almost all cases were severe, despite the simulation initially starting with both a mild and severe case. The dominance of severe disease was due to it being more transmissible and having a longer infectious period. I went on to explore how much more transmissible severe disease needs to be to dominate infections when $\alpha = 1$ (Fig. S3). For $R_0 = 1.1$, 99% of infections were severe when $\beta_S = 1.03\beta_M$. For higher values of R_0, a larger value of β_S was required for severe disease to completely dominate. For example, when $\beta_S = 1.1\beta_M$, 94% and 88% of cases were severe for $R_0 = 2.0$ and 3.0 respectively.

When considering the proportion of the population infected at the peak of the outbreak (Fig. 4(b)), I found that the proportion of cases that were severe followed a similar trend to the proportion infected (Fig. 4(a)). However, the proportion of the population infected at the outbreak's peak was higher for values of $\alpha > 0.5$, especially for larger values of R_0.

Although the total proportion of the population infected seemed roughly equal across α, the total proportion infected did in fact vary (Fig. 5, top row). Across all three values of R_0, the total proportion infected reached a minimum close to $\alpha = 0.5$ with the number of infections at that point decreasing from the expected final size by 0.22%, 0.79% and 0.54% for $R_0 = 1.1, 2.0$ and 3.0 respectively. In a population the size of the UK (67 million people), this is equivalent to a reduction of 147,000, 529,000 and 362,000 infections.

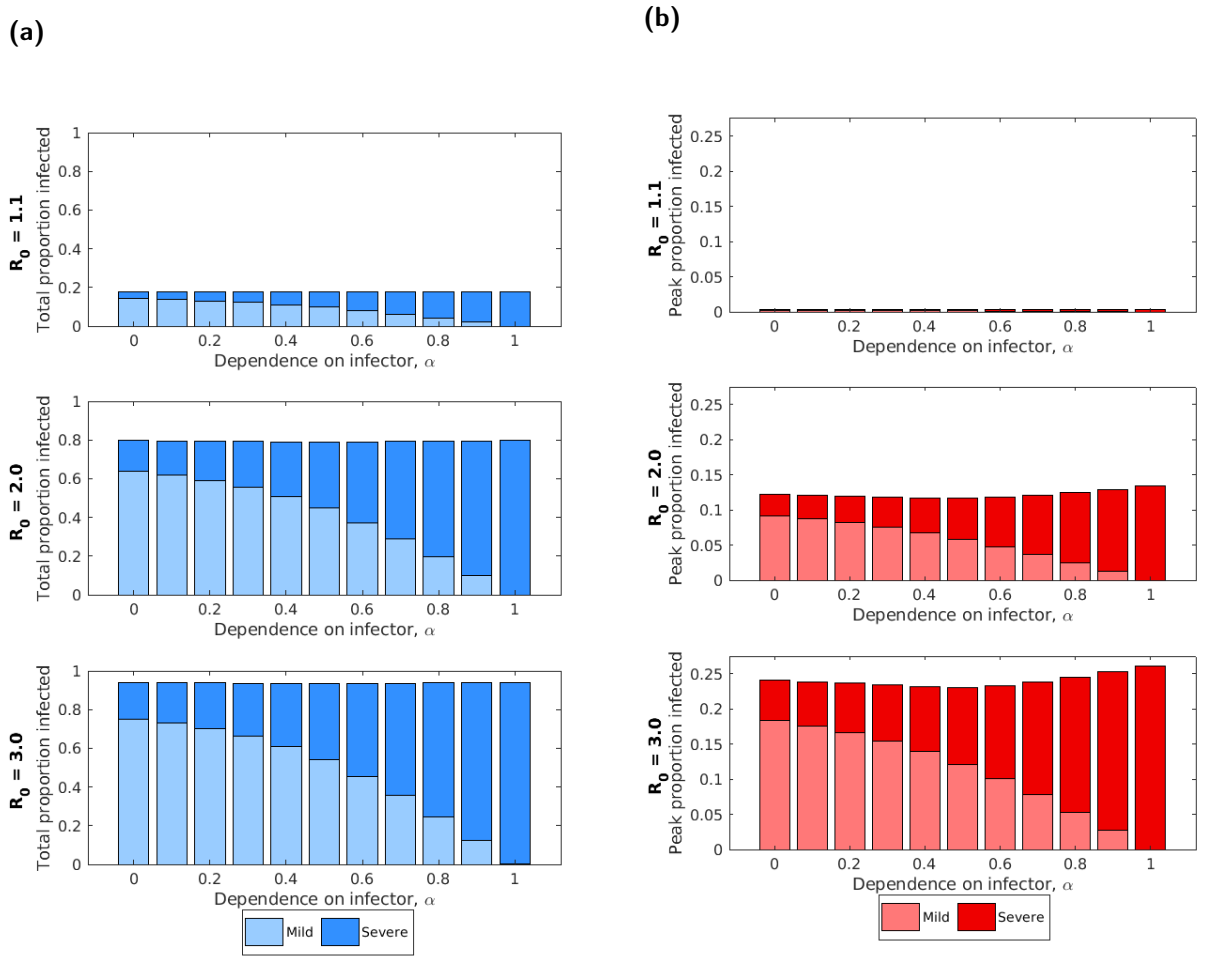

Figure 4: Investigating the total and peak proportion of the population infected for three values of R_0 whilst varying the dependence on the infector's symptom severity, α I present (a) the proportion of the population infected across the entire simulation and (b) the proportion of the population infected at the peak of the outbreak. The intensity of the shading denotes the symptom severity level with the darker colour showing severe infections and the lighter colour showing mild infections. The parameters are as given in Table 1 ($\nu = 0.2$, $\gamma_M = 1/5$, $\gamma_S = 1/7$ and $\beta_S/\beta_M = 2$).

From the results shown in Fig. 5 I expected the peak proportion infected to reduce to a minimum near $\alpha = 0.5$, as the number of infections has decreased. Interestingly, there was a much larger increase than expected in the peak proportion infected when $\alpha = 1$ due to the prevalence of severe cases and their increased infectious durations (Fig. 5, bottom row).

These results are supported by the temporal plots (Fig. S4) which showed that the peak in infections was noticeably larger for $\alpha = 1$. This plot also showed how the relative contribution from mild disease decreases with α.

Changing the severe infectious duration led to the total infections varying with α

To isolate the effect of severe and mild disease having different infectious durations, I set their transmission rates to be equal ($\beta_S/\beta_M = 1$) and then varied γ_S whilst keeping $\gamma_M = 1/5$ (Fig. 6). When $\gamma_S = \gamma_M = 1/5$, changing the dependence on the infector's symptom severity, α, has no effect on the total proportion of the population infected, which remains equal to the expected value. When γ_S was decreased (meaning the infectious duration was increased), the total proportion infected decreases to a minimum for some value of α but was equal to the expected value at $\alpha = 0$

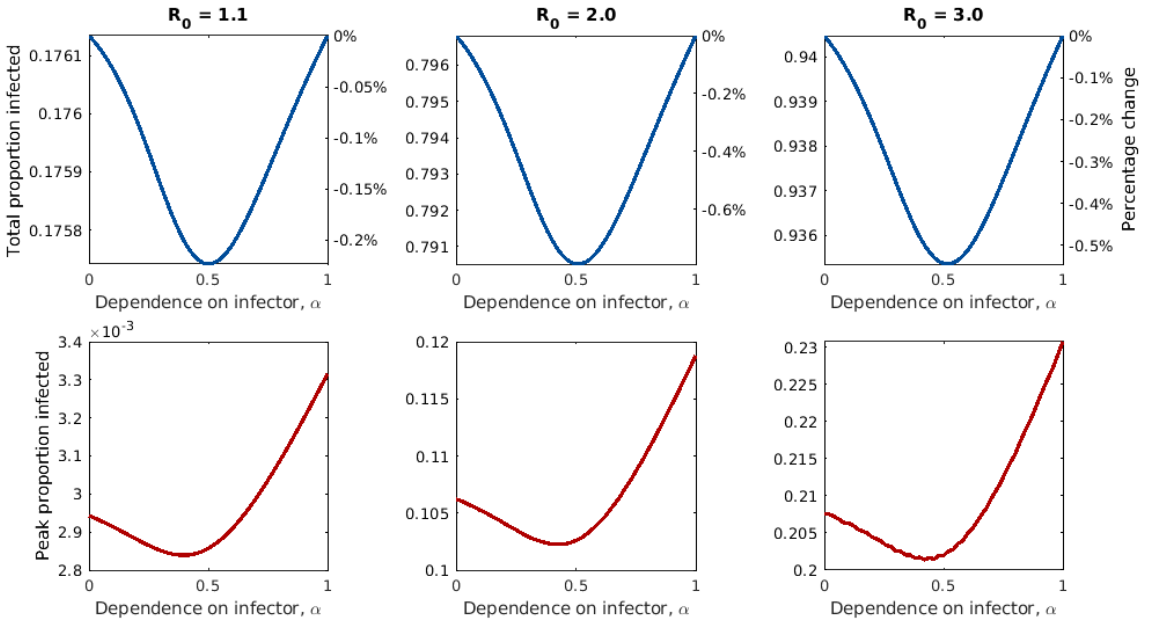

Figure 5: Investigating the total and peak proportion of the population infected over the entire simulation for three values of R_0 whilst varying the dependence on the infector's symptom severity, α. The first row shows the total proportion of the population infected in both severity classes varies compared to the calculated theoretical value for that value of R_0 which is shown by the dashed grey line. The second row shows the proportion of the population infected at the outbreak's peak across both severity classes. Note that the y scale varies across these plots since the change due to α was relatively small compared to the change due to R_0.

or 1. The value of α at which this minimum was attained and the percentage reduction in cases from the expected value varied with R_0 and γ_S.

I found that smaller values of γ_S (longer infectious period) led to the minimum occurring at lower values of α (Fig. 6). This relationship can be seen for all three values of R_0. When $R_0 = 2.0$ or 3.0, γ_S also strongly affects the percentage reduction from the expected value at the minimum point, with smaller values of γ_S leading to a larger percentage reduction of up to 2.5% (1,675,000 infections) and 1.8% (1,206,000 infections) for the two values of R_0. Contrastingly, when $R_0 = 1.1$, I found that γ_S had a minimal impact on the percentage reduction of people infected at the minimum which remained close to 0.7% (469,000 infections) for all values.

Inspecting the proportion of cases that are severe, I observed that it increased with α (Fig. 6, bottom row). I also found that the point at which there were equal numbers of mild and severe cases roughly lined up with the value of α for which the total proportion of the population infected attains its minimum.

Changing the transmission rate ratio has a limited effect on the total infections

To isolate the effect of severe disease being more transmissible than mild disease, I set the infectious periods to be equal ($\gamma_S = \gamma_M = 1/5$) and varied β_S/β_M whilst keeping the value of R_0 fixed (Fig. 7).

I found that, in general, the impact of changing β_S/β_M was minimal when compared to the impact of changing γ_S. The only noticeable change in the total proportion of the population infected was when $\beta_S/\beta_M = 1.1$ and α was close to one. However, even at this point, the percentage reduction from the expected value was less than 0.4%.

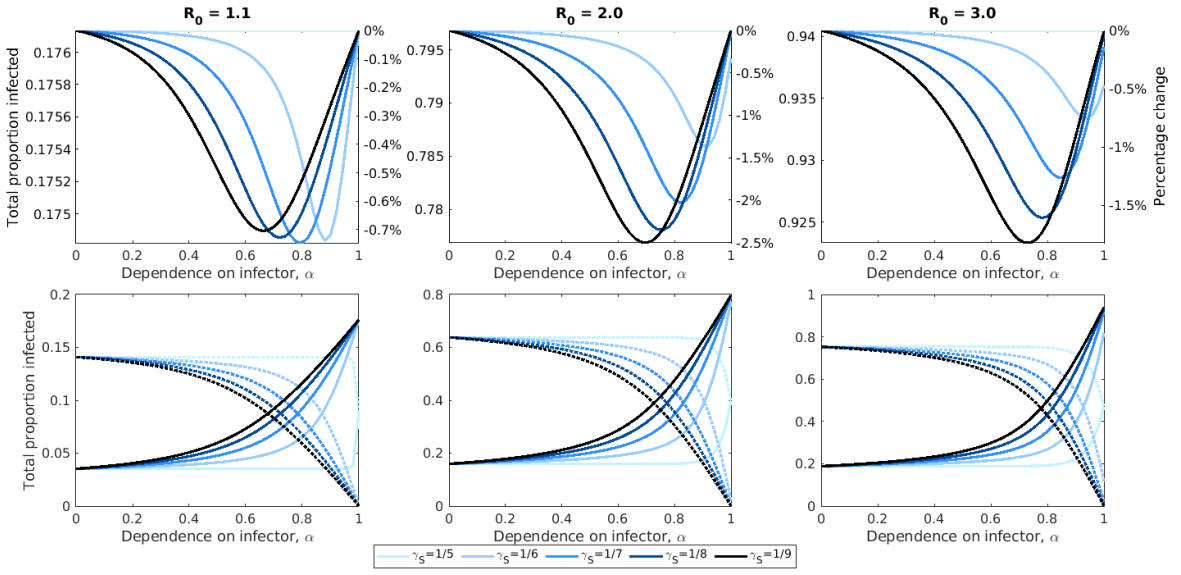

Figure 6: Investigating how the total proportion of the population infected changes as the infectious period for severe disease increases for three values of R_0 whilst varying the dependence on the infector's symptom severity. The first row shows the total proportion of the population infected across both symptom severity classes, with the right axis showing the percentage change from the calculated theoretical value. The second row shows the total proportion infected across both symptom severity classes with the dotted line showing mild infections and the solid line showing severe infections. Here β_S/β_M was assumed to be 1, $\nu = 0.2$ and $\gamma_M = 1/5$. For each value of γ_S and α, the value of β required to give the fixed value of R_0 was recalculated. The intensity of the shading denotes the severe recovery rate, γ_S, with darker colours referring to smaller values of γ_S (and therefore a longer infectious period). Note that the y-axis scale varies across these plots.

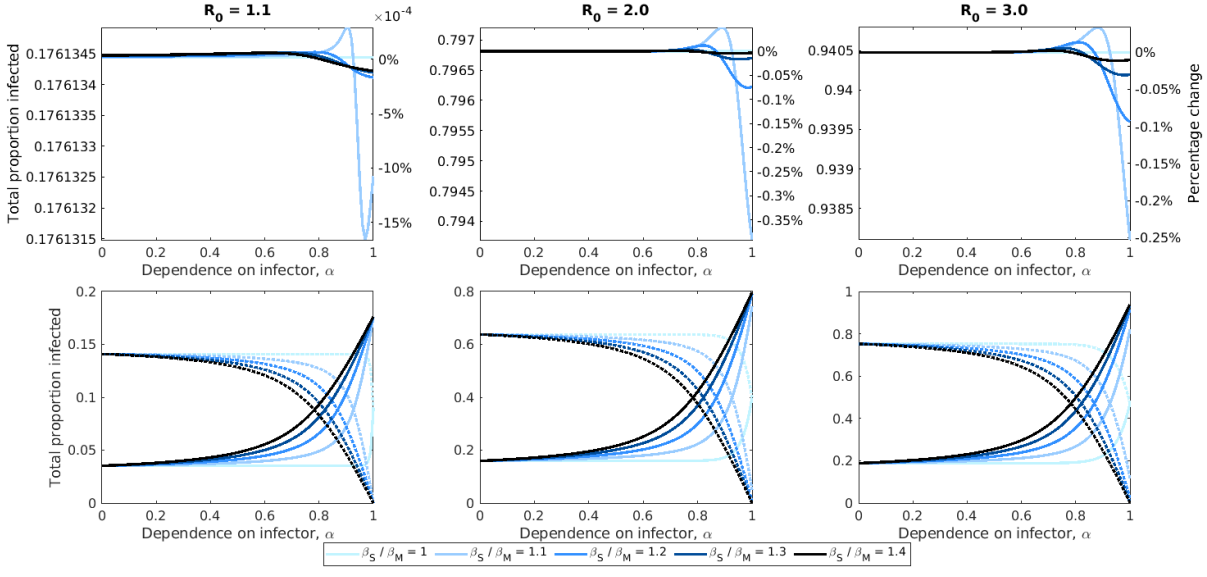

Figure 7: Investigating how the total proportion of the population infected changes as the ratio of transmission rates increases for three values of R_0 whilst varying the dependence on the infector's symptom severity. The first row shows the total proportion of the population infected across both symptom severity classes, with the right axis showing the percentage change from the calculated theoretical final outbreak size. The second row shows the total proportion infected across both symptom severity classes, with the dotted line showing mild infections and the solid line showing severe infections. Here $\nu = 0.2$ and $\gamma_M = \gamma_S = 1/5$. For each value of β_S/β_M and α, the value of β required to give the fixed value of R_0 required was recalculated. The intensity of the shading denotes the severe recovery rate, γ_S, with darker colours referring to smaller values of γ_S (and therefore a longer infectious period). Note that the y-axis scale varies across these plots.

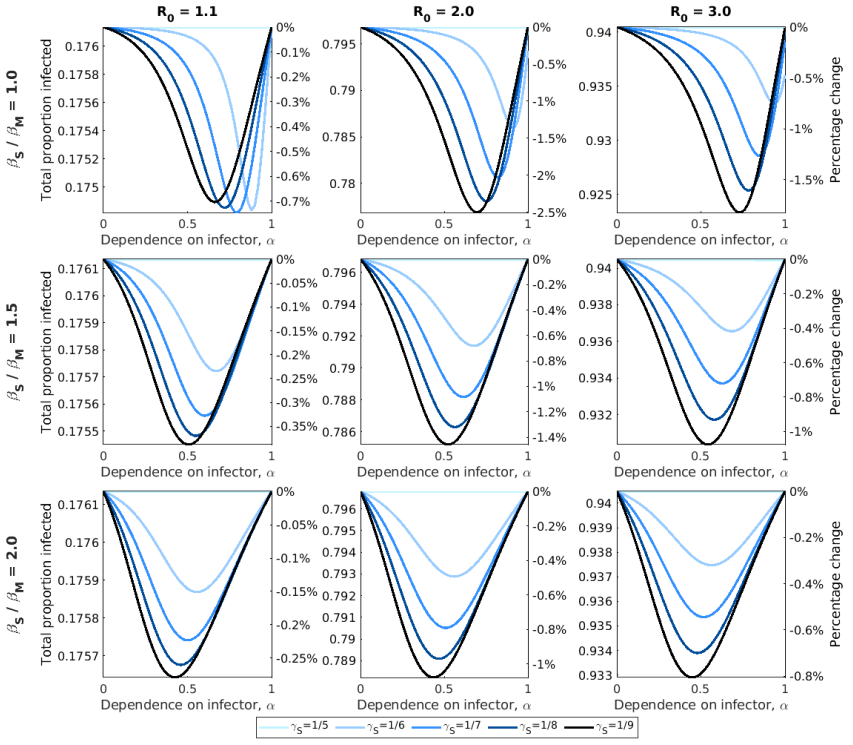

Figure 8: Investigating how the proportion of the population infected changes as β_S/β_M and γ_S increase simultaneously whilst varying α. The intensity of the shading denotes the severe recovery rate γ_S. Note that the y-axis scale varies across these plots.

I went on to explore the impact of changing γ_S and β_S/β_M simultaneously (Fig. 8). I found that increasing β_S/β_M when $\gamma_S > \gamma_M$ led to the minimum proportion of the population infected occurring at a lower value of α with a decreased percentage reduction from the expected final size.

Overall, I found that the difference in infectious periods for mild and severe disease was responsible for reducing the total proportion of the population infected for certain values of α. I hypothesised that this occurs because the increase in γ_S leads to a larger proportion of the cases being severe. One would then expect this to be amplified by the partial symptom severity mapping. However, the increase in severe cases mostly occurs near the end of the outbreak when the majority of mild cases have recovered but severe cases have not. This means that the increase in severe cases was not amplified, as by that point relatively few individuals are being infected. So the proportion of cases that are severe, and therefore the value of R_0, was overestimated for that parameter set (see Supporting Information S5 for a further explanation).

3.4. Exploring the effect of a symptom blocking intervention

Having so far explored the symptom severity model to gain an understanding of its transmission dynamics, I next investigated the effect of an intervention with a symptom-reducing effect. I explored how the dependence on the infector's symptom severity, α, impacted epidemiological outputs (total infections, severe infections and hospitalisations) and the cost-effectiveness of the intervention. The following plots show the epidemiological outputs as the number of infections or hospitalisations prevented (compared to the no intervention scenario) as a proportion of the total population size.

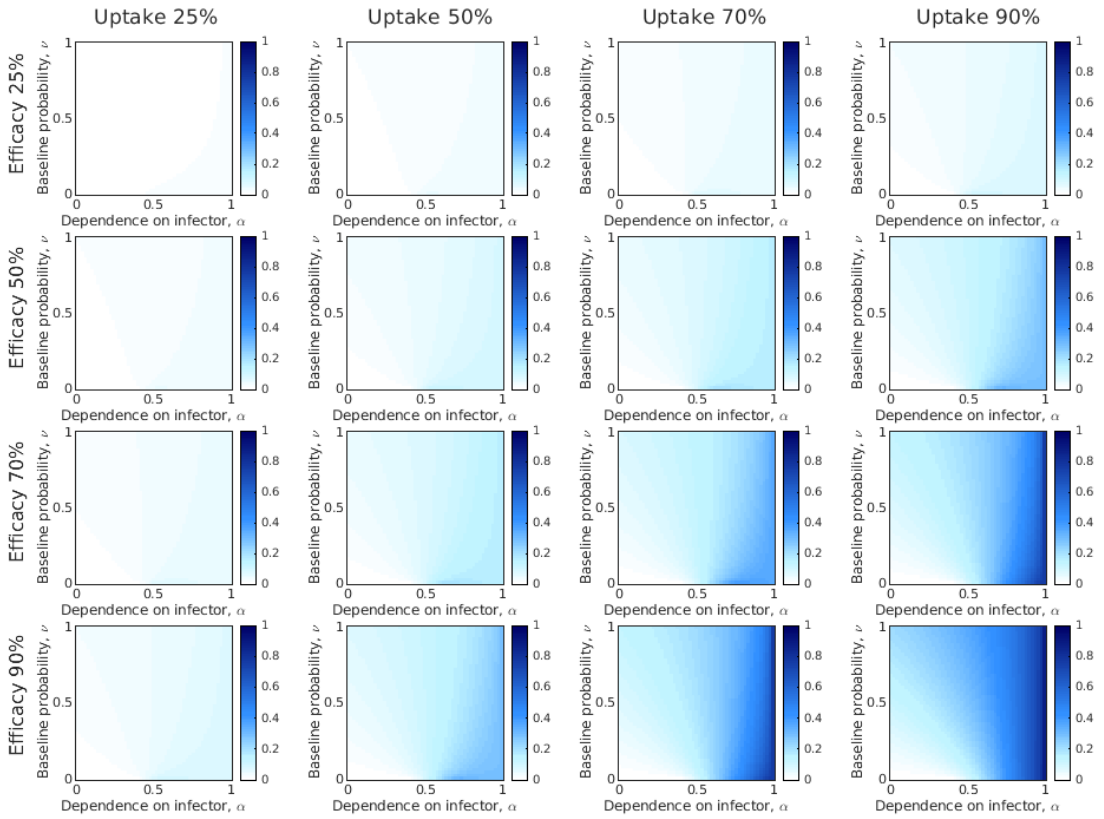

Figure 9: Investigating the number of infections prevented by the intervention as a proportion of the total population. For each uptake and efficacy and values of ν and α, the total number of infections at the end of the simulation are subtracted from the total number of infections in the no intervention scenario for those values of ν and α to give the number of infections prevented. This value was then divided by the total population size. The darker shading corresponds to a larger reduction in the proportion of the population infected.

Note that the model only depends on ηu where η is the efficacy and u is the uptake. This means that all the epidemiological outputs (Fig. 9, Fig. 10 and Fig. 11) are diagonally symmetrical; for example, the scenarios with efficacy of 70% and uptake of 50% are equivalent to the scenarios with efficacy of 50% and uptake of 70%.

Higher values of α led to the intervention preventing more infections

The effect of the uptake and efficacy on the number of infections prevented for different values of α and ν was shown in Fig. 9. When the uptake or efficacy was low (equal to 25%), the intervention prevented relatively few infections and the number of infections prevented was similar across different values of ν and α. When the uptake and efficacy were increased, α strongly impacted the number of infections prevented, with the intervention being much more effective for values of α close to 1. Therefore, increasing the uptake of the intervention had a much larger impact for values of α close to 1 than it did for values of α approaching 0. In general, ν had a minimal impact on the number of infections prevented by the intervention, except for when the uptake and efficacy were both at 90% where the intervention became more effective at preventing infections when ν was closer to 1.

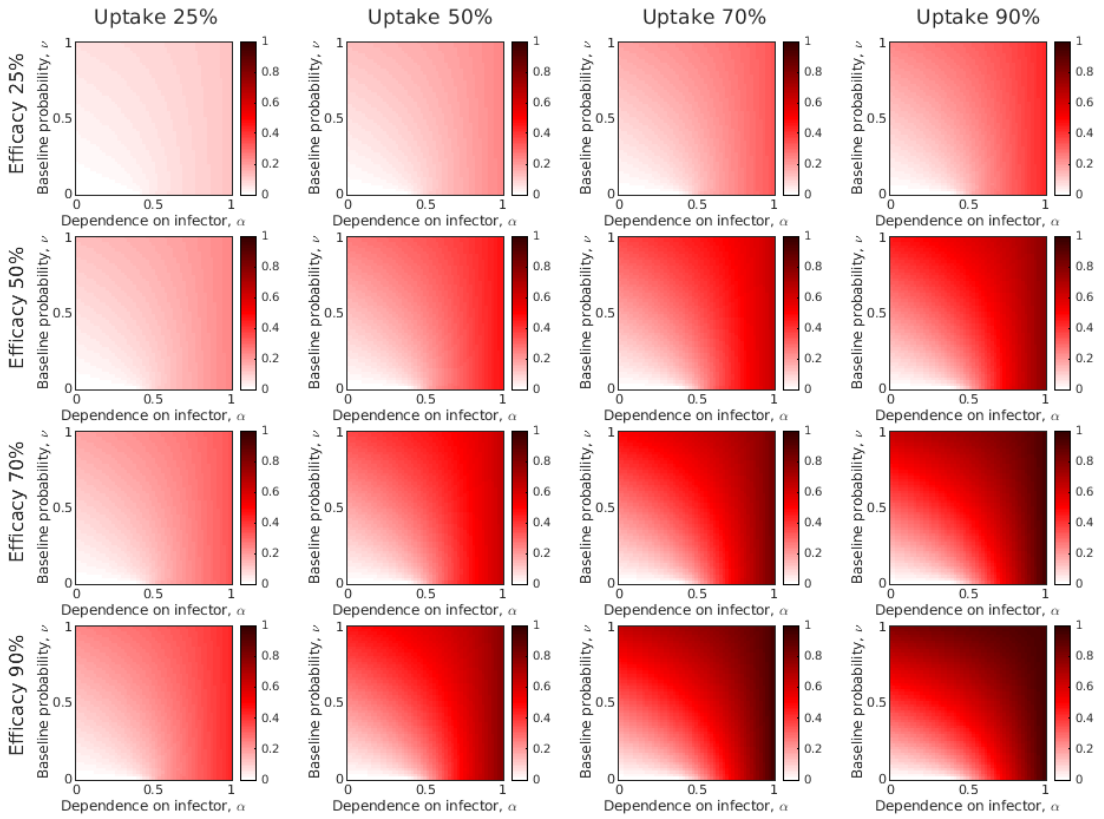

Figure 10: Investigating the number of severe infections prevented by the intervention as a proportion of the total population. For each uptake and efficacy and values of ν and α, the total number of severe infections at the end of the simulation are subtracted from the total number of severe infections in the no intervention scenario for those values of ν and α to give the number of severe infections prevented. This value was then divided by the total population size. The darker shading corresponds to a larger reduction in the proportion of the population infected with severe disease.

Higher values of α and ν led to the intervention preventing more severe infections

As with the total number of infections prevented (Fig. 9), the intervention's effectiveness at preventing severe infections depended strongly on α with more severe infections being prevented for α close to one (Fig. 10. When α was close to 1, increasing the uptake had a much larger impact on the number of severe cases prevented. When α was close to 0, increasing the uptake had a more limited effect.

In contrast, ν did have a larger effect on the number of severe cases prevented than it did on the total cases prevented. For high uptake or efficacy (70% or 90%), ν was as important as α when determining the number of severe cases prevented. This increase in the number of severe cases prevented was primarily due to there being a larger number of severe cases for these values of α and ν. When considering the percentage of severe cases prevented (Fig. S6), there was minimal dependence on both α and ν. Instead, the proportion of severe cases prevented was almost entirely dependent on the uptake and efficacy of the intervention.

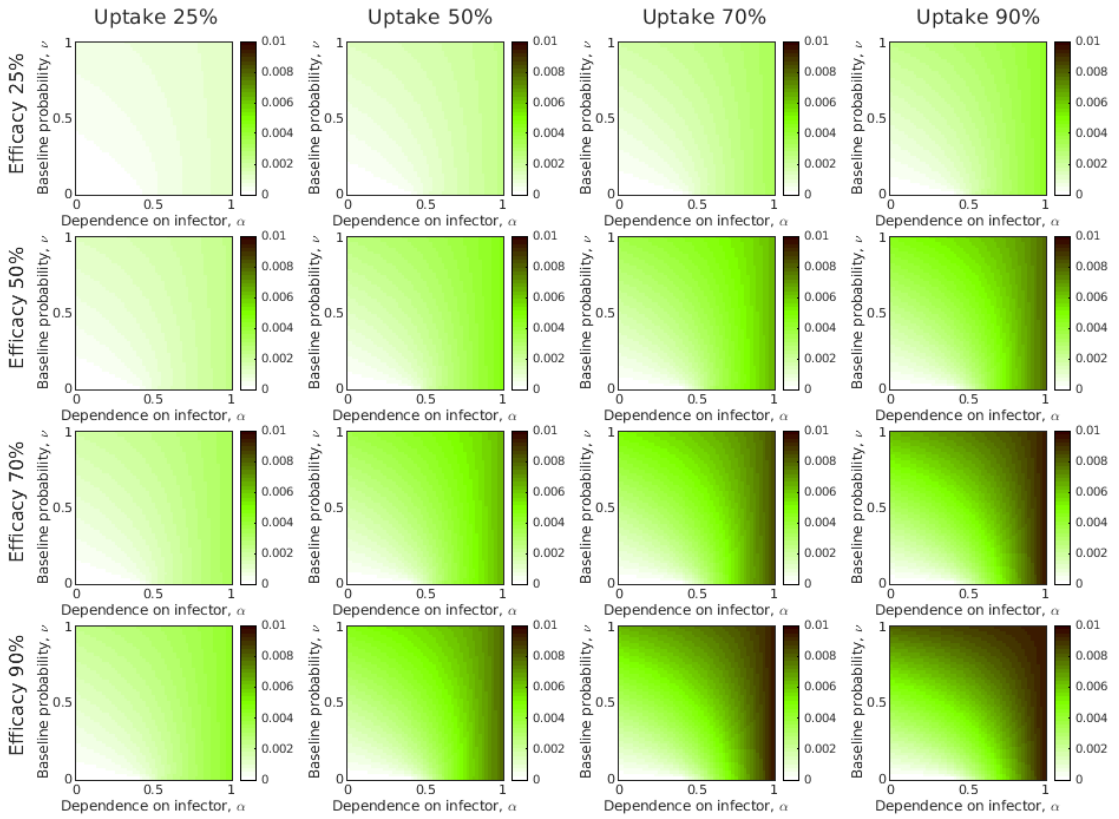

Figure 11: Investigating the number of hospitalisations prevented by the intervention as a proportion of the total population. For each uptake and efficacy and values of ν and α, the total number of hospitalisations at the end of the simulation are subtracted from the total number of hospitalisations in the no intervention scenario for those values of ν and α to give the number of hospitalisations prevented. This value was then divided by the total population size. The darker shading corresponds to a larger reduction in the proportion of the population hospitalised.

Higher values of α and ν led to the intervention preventing more hospitalisations

When considering the number of hospitalisation prevented by the intervention (Fig. 11), α and ν had a large impact on the number of hospitalisations prevented. When α or ν were close to 1 leading, there was a much greater reduction in hospitalisations. Unlike when considering the proportion of severe cases prevented (Fig. S6), α still had a large impact on the proportion of hospitalisations prevented when either uptake or efficacy was greater than 50% (Fig. S7). An exception was when uptake and efficacy were both 90%, where almost all hospitalisations were prevented regardless of the value of α.

Overall, the effectiveness of the intervention with a set uptake and efficacy was dependent on α and also ν, especially for α close to 0. When α or ν were close to 1, increasing the uptake substantially impacted the effectiveness, especially when the efficacy was high. However, for other values of α and ν, increasing the uptake had a minimal effect. Since the epidemiological outputs depended only on the value of ηu, where η was the efficacy and u was the uptake, increasing the efficacy for fixed uptake values gave the same relationship as described above.

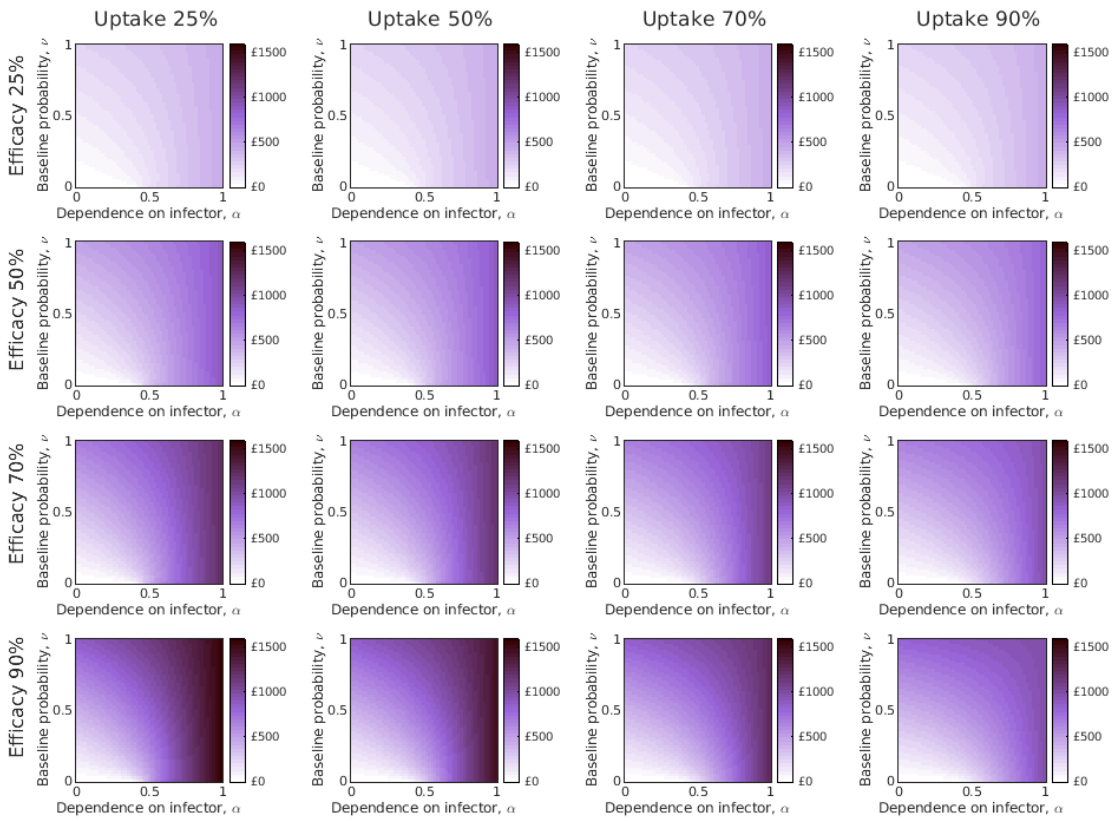

Figure 12: Investigating the threshold per unit intervention cost below which the intervention was cost-effective. The threshold per unit intervention cost was defined to be the per unit intervention cost at which the total cost of the intervention was equal to the willingness-to-pay per QALY gained multiplied by the number of QALYs gained. The darker shading corresponds to a larger threshold intervention cost.

Higher values of α and ν lead to a larger threshold intervention cost

The previous analysis showed that the intervention was more effective at preventing infections and hospitalisations when α or ν were close to one. This meant that, across all efficacy and uptake levels, the threshold per unit intervention cost was higher when α or ν were closer to one (Fig. 12).

The efficacy multiplied by the uptake controls the dynamics so an intervention with efficacy η and uptake of 100% was equivalent to an intervention with efficacy 2η and uptake 50% (or more generally efficacy $p\eta$ and uptake $\frac{100}{p}$%). Since these interventions are equivalent, one would be willing to pay the same overall cost and therefore would be willing to pay p times as much per unit of an intervention that was p times more effective. This relationship was reflected by the increase in the threshold per unit intervention cost as the efficacy increases (Fig. 12).

When the efficacy was relatively low (25% or 50%, first and second row in Fig. 12), the threshold per unit intervention cost remained relatively constant as the uptake was increased. However, when the efficacy was higher (70% or 90%, third and fourth row in Fig. 12), the threshold intervention cost was larger for lower uptake levels (25% or 50%) than it was for higher uptake levels (70% or 90%), especially when α was close to 1.

The optimal intervention uptake is highly sensitive to α when the efficacy is above 50%

Next, I explored the optimal intervention uptake for fixed values of α (0.0, 0.2, 0.5, 0.8, 1.0), ν (0.2, 0.5, 0.8) and the efficacy of the intervention (25%, 50%, 70%, 90%). This was motivated by the intervention uptake being a factor that public health policy can impact.

When looking at how the threshold intervention cost varies with the uptake (Fig. 13), the value of α greatly affected the qualitative relationship.

When $\alpha = 0.2$ (Fig. 13, top row), the threshold intervention cost increased with the uptake and the size of the increase depended on the efficacy and the value of ν. In general, the threshold intervention cost was low, reaching a maximum of £308 for this value of α.

When $\alpha = 0.5$ (Fig. 13, middle row), the relationship between the uptake and the threshold intervention cost was similar to when $\alpha = 0$ and the efficacy was low (25% or 50%). However, when the efficacy was high (70% or 90%), the threshold intervention cost decreased after a certain uptake level. This effect was especially noticeable when $\nu = 0.2$. When the efficacy was 90%, the threshold intervention cost reached a maximum of £379 at 30% uptake before decreasing to £290 at 100% uptake. In fact, the threshold intervention cost was lower at 100% uptake than at 1% uptake

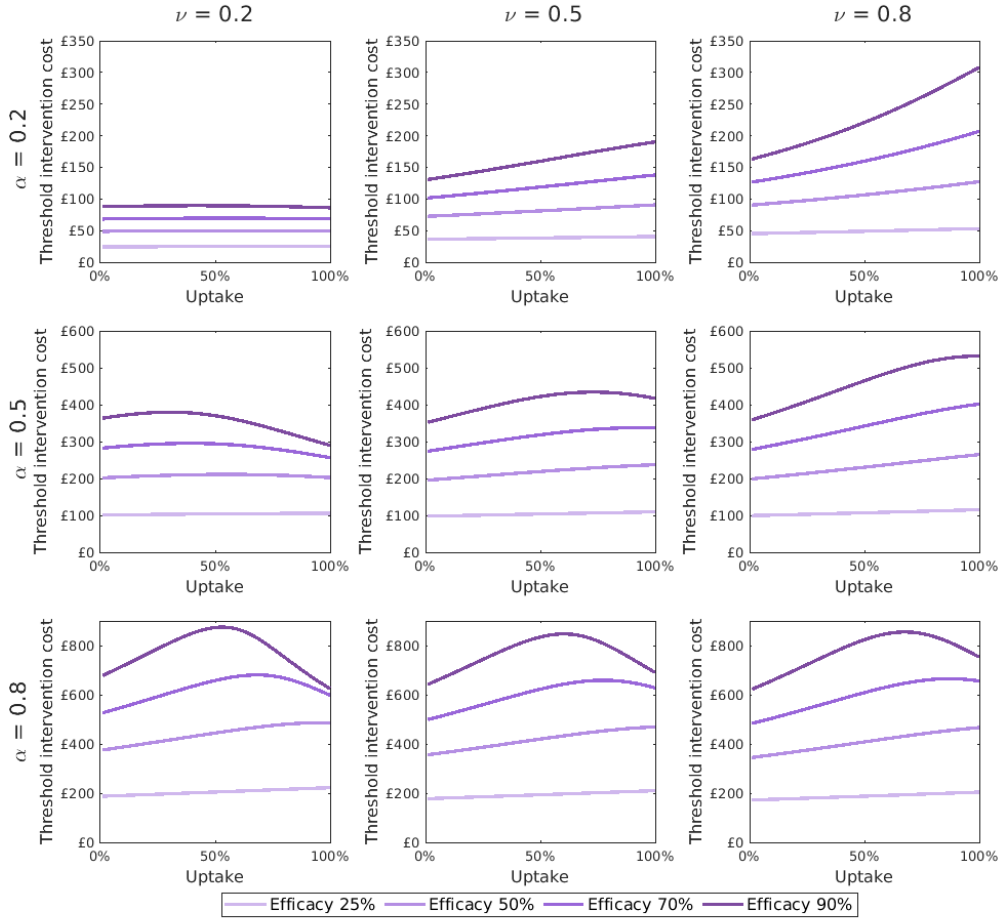

Figure 13: Investigating how the threshold per unit intervention cost varies with the uptake for different efficacies and values of α and ν.

(£290 vs £363). When the efficacy was 70%, I found a similar pattern with the threshold intervention cost increasing from £282 at 1% uptake to £295 at 39% uptake and then decreasing back to £256 at 100% uptake. Additionally, when the efficacy was 90%, the threshold intervention cost decreased from £433 at 73% uptake to £417 at 100% uptake when $\nu = 0.5$ and the threshold intervention cost stopped increasing when the uptake was close to 100% uptake for $\nu = 0.8$.

When $\alpha = 0.8$ (Fig. 13, bottom row), the value of ν had a minimal impact on the threshold intervention cost. When the efficacy was low (25% or 50%), the threshold intervention cost increased with the uptake. When the efficacy was 70% and $\nu = 0.2$, the threshold intervention cost peaked at £680 at 68% uptake before decreasing to £598 at 100% uptake. Similarly, when the efficacy was 90%, the threshold intervention cost peaked at £875 at 53% uptake before decreasing to £634 at 100% uptake.

In summary, the efficacy at which the 100% uptake was no longer optimal, and the optimal uptake for these larger efficacies, depended on the value of α and ν.

4. Discussion

Respiratory infections are a major focus in epidemiological and public health research. The COVID-19 pandemic has highlighted the importance of asymptomatic transmission with those exhibiting milder symptoms being included in many epidemiological models (Moghadas et al., 2020; Mathews et al., 2007). Despite this, there is still uncertainty around the transmission mechanisms of respiratory diseases and the relative contributions of different disease severities (Hall et al., 1979; Killingley and Nguyen-Van-Tam, 2013; Tellier, 2022)

Understanding the transmission mechanisms underpinning a symptom severity mapping for respiratory infections would allow governing bodies to use more effective intervention strategies that have the potential to save more lives and prevent spending more on less effective strategies.

I developed a generalisable framework that could capture multiple symptom severity levels which I used to explore the effect of a symptom severity mapping on epidemiological and health economic outcomes.

In the analytical exploration of R_0, I showed that the dependence on the infector's symptom severity (denoted by α) substantially impacted the value of R_0. This suggests that changing α would appreciably affect epidemiological outcomes and should be considered both when simulating from a given set of parameters and when estimating parameters from empirical data. Additionally, the dependence on the infector's symptom severity when the infector had severe disease (α_S) had a more considerable impact on R_0 than the dependence when the infector had mild disease (α_M). Although further work is required to establish the relative importance of α_S and α_M, my initial results suggest that research focusing on the onwards transmission of severe disease (for example, by focusing on transmission via aerosols) should be prioritised.

In the computational exploration the model's sensitivity to α, I found that the proportion of cases that were severe increased with α. This supports the findings of Paulo et al. (2010), who determined that the inclusion of a dose-response relationship led to an increased incidence of severe disease and a high mortality rate. In addition, when α was close to one (the dependence on the infector's symptom severity was high) the majority of cases were severe. When $\alpha = 1$, severe disease dominated the outbreak even when it was only slightly more transmissible. The dominance of severe disease could motivate the use of quarantining measures for those with severe disease early on during an outbreak. Although, such measures may be less effective if started once the outbreak is widespread unless the uptake is sufficiently high. Further research into quarantining measures with strategies focused on either severe disease or all infected individuals is required to establish its effectiveness for different strengths of symptom severity mappings.

In addition, I found that if severe disease had a longer infectious duration than mild disease, the total number of infections depended on the value of α even when R_0 was fixed across simulations. When there was partial dependence

on the infector's symptom severity, the total number of infections was lower than the theoretical final size. This suggests that α is an essential factor to consider when estimating the total number of infections from the value of R_0 or vice versa. Also, since the total number of infections depends on the difference in the severe and mild infectious periods, research into understanding their respective infectious periods is crucial to consider. The importance of infectious periods found in this report aligns with the results of Harris et al. (2022), who found that a symptom severity mapping exaggerated the effect of asymptomatic infections having a longer infectious period.

Across these computational results, R_0 had a minimal impact on the qualitative results suggesting that the general findings apply to a number of respiratory infections with a range of R_0 values.

Thirdly, I found that the cost-effectiveness of an intervention with a symptom-blocking effect was highly dependent on α. The intervention was most effective at preventing infections and hospitalisations when either the dependence on the infector's symptom severity, α, or the underlying probability of severe disease, ν, was high. This meant the intervention being most effective corresponded to when the proportion of cases that were severe was high. Therefore, even if a symptom severity mapping is not included, the use of separate symptom severity classes is vital to predicting the effectiveness of an intervention. Similarly, I found that the intervention was most cost-effective when α or ν were high. When investigating how the threshold intervention cost varied with the uptake for a fixed intervention efficacy and fixed values of α and ν, I found that the optimal uptake varied substantially with α. For α close to zero, 100% uptake was optimal. However, for larger α and high efficacies, the optimal uptake was less than 100%. This suggests that the optimal intervention strategy is potentially dependent on the value of α and that not including a symptom severity mapping during intervention analysis could lead to the use of a less cost-effective intervention strategy.

There are of course limitations to the work done in this report. I aimed to apply these results to general respiratory infections but have used data for influenza specifically to parameterise the model. As such, some of the underlying assumptions, such as severe disease having a longer infectious period than mild disease, may not apply to other respiratory infections of interest. In addition, the model used does not include any spatial heterogeneity. This could be vital in establishing the effectiveness of interventions and patterns that could allow a symptom severity mapping to be predicted from data; one such example would be an increase in clusters of severe disease. There is also uncertainty in the parameters used for the health economic modelling. Firstly, the analysis was only performed for $R_0 = 3.0$. Exploring a value of R_0 closer to one might lead to more variable results due to an increase in the likelihood of the intervention preventing the outbreak by reducing the effective reproductive ratio below one. The QALY loss values for the different disease severity levels also have much uncertainty, partly due to the lack of a formal scheme to define "severe" and "mild" disease. One assumption that could notably impact the intervention's cost-effectiveness is that mild disease leads to no QALY losses. This could lead to an underestimate of the effectiveness of an intervention that prevents a large number of mild cases. In addition, the WTP per QALY was assumed to be £20,000, but often analysis is performed using a WTP per QALY of £30,000. Using this value instead would lead to a higher threshold per unit intervention cost and potential intervention strategies being deemed cost-effective when they would not have been when the WTP per QALY was £20,000.

Whilst this report establishes the importance of a symptom severity mapping, further work is still required to fully determine its effect on epidemiological outcomes and the cost-effectiveness of interventions. One key inclusion would be separate age classes with different underlying probabilities of having severe disease. Intervention strategies that initially target specific age groups are widespread, leading to a focus on determining the optimal priority ordering as seen for vaccine strategies during the COVID-19 pandemic (Moore et al., 2021a,b). This research motivates the use of age classes when exploring intervention strategies since changing the priority order can have dramatic effects on public health outcomes. Age classes would also be important to include when determining the likelihood of a

symptom severity mapping from a data set, as age groups have different probabilities of severe disease and individuals have a higher likelihood of interacting with those of a similar age. Additional symptom severity classes could also be included, such as asymptomatic infections. The model could also be extended to account for symptom severity changing throughout the infection. Other intervention strategies, such as the quarantining measures mentioned earlier, would also be important to explore. One key extension to the work done in this report would be the exploration of a symptom severity mapping with both a symptom blocking and infection blocking effect.

There are still significant gaps in our understanding of the transmission of respiratory pathogens. More experimental data is required to understand the transmission routes, how symptoms develop after infection, and how and if symptom severity passes on with infection. This report motivates further research to continue enhancing our understanding of the importance of a symptom severity mapping on questions relevant to public health policy.

Acknowledgments

I thank Dr Edward Hill and Prof Matt Keeling for their expert supervision and insightful discussions. I also thank Dr Rebecca Mancy and Ciaran McMonagle from the University of Glasgow for their suggestions and help motivating the project and refining the research direction. Thanks to Dr Fergus Cumming and Dr Thomas Finnie from the UK Health Security Agency for their insights into future extensions of the project. This work was undertaken at the EPSRC CDT in Mathematics for Real-World Systems II, which is supported by the EPSRC grant EP/S022244/1.

References

Aaby, P., Coovadia, H., 1985. Severe measles: a reappraisal of the role of nutrition, overcrowding and virus dose. Medical hypotheses 18, 93–112. URL: https://pubmed.ncbi.nlm.nih.gov/3939698/, doi:10.1016/0306-9877(85)90042-8.

Al-Abdely, H.M., Midgley, C.M., Alkhamis, A.M., Abedi, G.R., Lu, X., Binder, A.M., Alanazi, K.H., Tamin, A., Banjar, W.M., Lester, S., Abdalla, O., Dahl, R.M., Mohammed, M., Trivedi, S., Algarni, H.S., Sakthivel, S.K., Algwizani, A., Bafaqeeh, F., Alzahrani, A., Alsharef, A.A., Alhakeem, R.F., Jokhdar, H.A., Ghazal, S.S., Thornburg, N.J., Erdman, D.D., Assiri, A.M., Watson, J.T., Gerber, S.I., 2019. Middle East Respiratory Syndrome Coronavirus Infection Dynamics and Antibody Responses among Clinically Diverse Patients, Saudi Arabia. Emerging Infectious Diseases 25, 753. URL: /pmc/articles/PMC6433025//pmc/articles/PMC6433025/?report=abstracthttps://www.ncbi.nlm.nih.gov/pmc/articles/PMC6433025/, doi:10.3201/EID2504.181595.

Aledort, J.E., Lurie, N., Wasserman, J., Bozzette, S.A., 2007. Non-pharmaceutical public health interventions for pandemic influenza: an evaluation of the evidence base. BMC Public Health 7, 208. doi:10.1186/1471-2458-7-208.

Andersson, J., 2021. What drives transmission of severe acute respiratory syndrome coronavirus 2? Journal of Internal Medicine 290, 949–951. doi:10.1111/joim.13335.

Apisarnthanarak, A., Mundy, L.M., 2010. Outbreak of Influenza A (2009) H1N1 among Thai Healthcare Workers: Is It Time to Integrate a Vaccination Program? Infection Control & Hospital Epidemiology 31, 854–856. doi:10.1086/655019.

Appleby, J., 2022. The public finance cost of COVID-19. BMJ 376. URL: https://www.bmj.com/content/376/bmj.o490https://www.bmj.com/content/376/bmj.o490.abstract, doi:10.1136/BMJ.O490.

Atkinson, M.P., Wein, L.M., 2008. Quantifying the Routes of Transmission for Pandemic Influenza. Bulletin of Mathematical Biology 70, 820–867. doi:10.1007/s11538-007-9281-2.

Awofeso, N., Fennell, M., Waliuzzaman, Z., O'Connor, C., Pittam, D., Boonwaat, L., de Kantzow, S., Rawlinson, W.D., 2001. Influenza outbreak in a correctional facility. Australian and New Zealand Journal of Public Health 25, 443–446. doi:10.1111/j.1467-842X.2001.tb00290.x.

Bjornson, A.B., Mellencamp, M.A., Schiff, G.M., 1991. Complement Is Activated in the Upper Respiratory Tract during Influenza Virus Infection. American Review of Respiratory Disease 143, 1062–1066. doi:10.1164/ajrccm/143.5{_}Pt{_}1.1062.

Bodewes, R., Kreijtz, J.H., van Amerongen, G., Fouchier, R.A., Osterhaus, A.D., Rimmelzwaan, G.F., Kuiken, T., 2011. Pathogenesis of Influenza A/H5N1 Virus Infection in Ferrets Differs between Intranasal and Intratracheal Routes of Inoculation. The American Journal of Pathology 179, 30–36. doi:10.1016/j.ajpath.2011.03.026.

Brankston, G., Gitterman, L., Hirji, Z., Lemieux, C., Gardam, M., 2007. Transmission of influenza A in human beings. The Lancet Infectious Diseases 7, 257–265. doi:10.1016/S1473-3099(07)70029-4.

Cao, B., Li, X.W., Mao, Y., Wang, J., Lu, H.Z., Chen, Y.S., Liang, Z.A., Liang, L., Zhang, S.J., Zhang, B., Gu, L., Lu, L.H., Wang, D.Y., Wang, C., 2009. Clinical Features of the Initial Cases of 2009 Pandemic Influenza A (H1N1) Virus Infection in China. New England Journal of Medicine 361, 2507–2517. doi:10.1056/NEJMoa0906612.

Carrat, F., Vergu, E., Ferguson, N.M., Lemaitre, M., Cauchemez, S., Leach, S., Valleron, A.J., 2008. Time Lines of Infection and Disease in Human Influenza: A Review of Volunteer Challenge Studies. American Journal of Epidemiology 167, 775–785. doi:10.1093/aje/kwm375.

Centers for Disease Control and Prevention, 2019. 1918 Pandemic (H1N1 virus). URL: https://www.cdc.gov/flu/pandemic-resources/1918-pandemic-h1n1.html.

Centers for Disease Control and Prevention, 2021. Plague. URL: https://www.cdc.gov/plague/index.html.

Chu, C.M., Poon, L.L., Cheng, V.C., Chan, K.S., Hung, I.F., Wong, M.M., Chan, K.H., Leung, W.S., Tang, B.S., Chan, V.L., Ng, W.L., Sim, T.C., Ng, P.W., Law, K.I., Tse, D.M., Peiris, J.S., Yuen, K.Y., 2004. Initial viral load and the outcomes of SARS. CMAJ : Canadian Medical Association Journal 171, 1349. URL: /pmc/articles/PMC527336//pmc/articles/PMC527336/?report=abstracthttps://www.ncbi.nlm.nih.gov/pmc/articles/PMC527336/, doi:10.1503/CMAJ.1040398.

Couch, R.B., Gordon Douglas, R., Fedson, D.S., Kasel, J.A., 1971. Correlated Studies of a Recombinant Influenza-Virus Vaccine. III. Protection against Experimental Influenza in Man. Journal of Infectious Diseases 124, 473–480. doi:10.1093/infdis/124.5.473.

Cowling, B.J., Ip, D.K.M., Fang, V.J., Suntarattiwong, P., Olsen, S.J., Levy, J., Uyeki, T.M., Leung, G.M., Malik Peiris, J.S., Chotpitayasunondh, T., Nishiura, H., Mark Simmerman, J., 2013. Aerosol transmission is an important mode of influenza A virus spread. Nature Communications 4, 1935. doi:10.1038/ncomms2922.

Cromer, D., van Hoek, A.J., Jit, M., Edmunds, W.J., Fleming, D., Miller, E., 2014. The burden of influenza in England by age and clinical risk group: A statistical analysis to inform vaccine policy. Journal of Infection 68, 363–371. doi:10.1016/j.jinf.2013.11.013.

Dattorro, J., 2006. Convex Optimization and Euclidean Distance Geometry.

Dawood, F.S., Iuliano, A.D., Reed, C., Meltzer, M.I., Shay, D.K., Cheng, P.Y., Bandaranayake, D., Breiman, R.F., Brooks, W.A., Buchy, P., Feikin, D.R., Fowler, K.B., Gordon, A., Hien, N.T., Horby, P., Huang, Q.S., Katz, M.A., Krishnan, A., Lal, R., Montgomery, J.M., Mølbak, K., Pebody, R., Presanis, A.M., Razuri, H., Steens, A., Tinoco, Y.O., Wallinga, J., Yu, H., Vong, S., Bresee, J., Widdowson, M.A., 2012. Estimated global mortality associated with the first 12 months of 2009 pandemic influenza A H1N1 virus circulation: a modelling study. The Lancet Infectious Diseases 12, 687–695. URL: http://www.thelancet.com/article/S1473309912701214/fulltexthttp://www.thelancet.com/article/S1473309912701214/abstracthttps://www.thelancet.com/journals/laninf/article/PIIS1473-3099(12)70121-4/abstract, doi:10.1016/S1473-3099(12)70121-4.

Dean, K.R., Krauer, F., Walløe, L., Lingjærde, O.C., Bramanti, B., Stenseth, N.C., Schmid, B.V., 2018. Human ectoparasites and the spread of plague in Europe during the Second Pandemic. Proceedings of the National Academy of Sciences 115, 1304–1309. doi:10.1073/pnas.1715640115.

Diekmann, O., Heesterbeek, J., Metz, J., 1990. On the definition and the computation of the basic reproduction ratio R 0 in models for infectious diseases in heterogeneous populations. Journal of Mathematical Biology 28. doi:10.1007/BF00178324.

Drancourt, M., Houhamdi, L., Raoult, D., 2006. Yersinia pestis as a telluric, human ectoparasite-borne organism. The Lancet Infectious Diseases 6, 234–241. doi:10.1016/S1473-3099(06)70438-8.

Forum of International Respiratory Societies, 2021. The global impact of respiratory disease. European Respiratory Society URL: firsnet.org/images/publications/FIRS_Master_09202021.pdf.

Gani, R., Leach, S., 2004. Epidemiologic Determinants for Modeling Pneumonic Plague Outbreaks. Emerging Infectious Diseases 10, 608–614. doi:10.3201/eid1004.030509.

González López-Valcárcel, B., Vallejo-Torres, L., 2020. The costs of COVID-19 and the cost-effectiveness of testing. Applied Economic Analysis 29, 77–89. doi:10.1108/AEA-11-2020-0162/FULL/PDF.

Hall, C.B., Douglas, R.G., Geiman, J.M., Meagher, M.P., 1979. Viral Shedding Patterns of Children with Influenza B Infection. Journal of Infectious Diseases 140, 610–613. doi:10.1093/infdis/140.4.610.

Han, A., Czajkowski, L.M., Donaldson, A., Baus, H.A., Reed, S.M., Athota, R.S., Bristol, T., Rosas, L.A., Cervantes-Medina, A., Taubenberger, J.K., Memoli, M.J., 2019. A Dose-finding Study of a Wild-type Influenza A(H3N2) Virus in a Healthy Volunteer Human Challenge Model. Clinical Infectious Diseases: An Official Publication of the Infectious Diseases Society of America 69, 2082. URL: /pmc/articles/PMC6880340//pmc/articles/PMC6880340/?report=abstracthttps://www.ncbi.nlm.nih.gov/pmc/articles/PMC6880340/, doi:10.1093/CID/CIZ141.

Harris, J.D., Woo Park, S., Dushoff, J., Weitz, J.S., 2022. How time-scale differences in asymptomatic and symptomatic transmission shape SARS-CoV-2 outbreak dynamics URL: https://doi.org/10.1101/2022.04.21.22274139, doi:10.1101/2022.04.21.22274139.

Herlocher, M., Elias, S., Truscon, R., Harrison, S., Mindell, D., Simon, C., Monto, A., 2001. Ferrets as a Transmission Model for Influenza: Sequence Changes in HA1 of Type A (H3N2) Virus. The Journal of Infectious Diseases 184, 542–546. doi:10.1086/322801.

Hill, E.M., Petrou, S., Forster, H., de Lusignan, S., Yonova, I., Keeling, M.J., 2020. Optimising age coverage of seasonal influenza vaccination in England: A mathematical and health economic evaluation. PLOS Computational Biology 16, e1008278. URL: https://dx.plos.org/10.1371/journal.pcbi.1008278, doi:10.1371/journal.pcbi.1008278.

Hollmann, M., Garin, O., Galante, M., Ferrer, M., Dominguez, A., Alonso, J., 2013. Impact of Influenza on Health-Related Quality of Life among Confirmed (H1N1)2009 Patients. PLoS ONE 8. URL: /pmc/articles/PMC3610925//pmc/articles/PMC3610925/?report=abstracthttps://www.ncbi.nlm.nih.gov/pmc/articles/PMC3610925/, doi:10.1371/JOURNAL.PONE.0060477.

Imai, M., Iwatsuki-Horimoto, K., Hatta, M., Loeber, S., Halfmann, P.J., Nakajima, N., Watanabe, T., Ujie, M., Takahashi, K., Ito, M., Yamada, S., Fan, S., Chiba, S., Kuroda, M., Guan, L., Takada, K., Armbrust, T., Balogh, A., Furusawa, Y., Okuda, M., Ueki, H., Yasuhara, A., Sakai-Tagawa, Y., Lopes, T.J.S., Kiso, M., Yamayoshi, S., Kinoshita, N., Ohmagari, N., Hattori, S.i., Takeda, M., Mitsuya, H., Krammer, F., Suzuki, T., Kawaoka, Y., 2020. Syrian hamsters as a small animal model for SARS-CoV-2 infection and countermeasure development. Proceedings of the National Academy of Sciences 117, 16587–16595. doi:10.1073/pnas.2009799117.

Jones, R.M., Su, Y.M., 2015. Dose-response models for selected respiratory infectious agents:, group a, rhinovirus and respiratory syncytial virus. BMC Infectious Diseases 15, 1–9. URL: https://bmcinfectdis.biomedcentral.com/articles/10.1186/s12879-015-0832-0, doi:10.1186/S12879-015-0832-0/TABLES/1.

Karimzadeh, S., Bhopal, R., Nguyen Tien, H., 2021. Review of infective dose, routes of transmission and outcome of COVID-19 caused by the SARS-COV-2: comparison with other respiratory viruses– CORRIGENDUM. Epidemiology and Infection 149, e116. doi:10.1017/S0950268821001084.

Killingley, B., Nguyen-Van-Tam, J., 2013. Routes of influenza transmission. Influenza and Other Respiratory Viruses 7, 42–51. doi:10.1111/irv.12080.

Kohli, M., Maschio, M., Becker, D., Weinstein, M.C., 2021. The potential public health and economic value of a hypothetical COVID-19 vaccine in the United States: Use of cost-effectiveness modeling to inform vaccination prioritization. Vaccine 39, 1157–1164. doi:10.1016/j.vaccine.2020.12.078.

Lelieveld, J., Helleis, F., Borrmann, S., Cheng, Y., Drewnick, F., Haug, G., Klimach, T., Sciare, J., Su, H., Pöschl, U., 2020. Model Calculations of Aerosol Transmission and Infection Risk of COVID-19 in Indoor Environments. International Journal of Environmental Research and Public Health 17, 8114. doi:10.3390/ijerph17218114.

Little, J.W., Gordon, R.D., Hall, W.J., Roth, F.K., 1979. Attenuated influenza produced by experimental intranasal inoculation. Journal of Medical Virology 3, 177–188. doi:10.1002/jmv.1890030303.

Lozano, R., Naghavi, M., Foreman, K., Lim, S., Shibuya, K., Aboyans, V., Abraham, J., Adair, T., Aggarwal, R., Ahn, S.Y., AlMazroa, M.A., Alvarado, M., Anderson, H.R., Anderson, L.M., Andrews, K.G., Atkinson, C., Baddour, L.M., Barker-Collo, S., Bartels, D.H., Bell, M.L., others, 2012. Global and regional mortality from 235 causes of death for 20 age groups in 1990 and 2010: a systematic analysis for the Global Burden of Disease Study 2010. The Lancet 380, 2095–2128. doi:10.1016/S0140-6736(12)61728-0.

Mathews, J.D., McCaw, C.T., McVernon, J., McBryde, E.S., McCaw, J.M., 2007. A Biological Model for Influenza Transmission: Pandemic Planning Implications of Asymptomatic Infection and Immunity. PLoS ONE 2, e1220. doi:10.1371/journal.pone.0001220.

Moghadas, S.M., Fitzpatrick, M.C., Sah, P., Pandey, A., Shoukat, A., Singer, B.H., Galvani, A.P., 2020. The implications of silent transmission for the control of COVID-19 outbreaks. Proceedings of the National Academy of Sciences 117, 17513–17515. doi:10.1073/pnas.2008373117.

Moore, S., Hill, E.M., Dyson, L., Tildesley, M.J., Keeling, M.J., 2021a. Modelling optimal vaccination strategy for SARS-CoV-2 in the UK. PLOS Computational Biology 17, e1008849. doi:10.1371/journal.pcbi.1008849.

Moore, S., Hill, E.M., Tildesley, M.J., Dyson, L., Keeling, M.J., 2021b. Vaccination and non-pharmaceutical interventions for COVID-19: a mathematical modelling study. The Lancet Infectious Diseases 21, 793–802. doi:10.1016/S1473-3099(21)00143-2.

Morawska, L., Cao, J., 2020. Airborne transmission of SARS-CoV-2: The world should face the reality. Environment International 139, 105730. doi:10.1016/j.envint.2020.105730.

Moser, M.R., Bender, T.R., Margolis, H.S., Noble, G.R., Kendal, A.P., Ritter, D.G., 1979. An outbreak of influenza aboard a commercial airliner. American Journal of Epidemiology 110, 1–6. doi:10.1093/oxfordjournals.aje.a112781.

National Health Service, 2019. SARS (severe acute respiratory syndrome). URL: https://www.nhs.uk/conditions/sars/.

Neilan, A.M., Losina, E., Bangs, A.C., Flanagan, C., Panella, C., Eskibozkurt, G.E., Mohareb, A., Hyle, E.P., Scott, J.A., Weinstein, M.C., Siedner, M.J., Reddy, K.P., Harling, G., Freedberg, K.A., Shebl, F.M., Kazemian, P., Ciaranello, A.L., 2021. Clinical Impact, Costs, and Cost-effectiveness of Expanded Severe Acute Respiratory Syndrome Coronavirus 2 Testing in Massachusetts. Clinical Infectious Diseases 73, e2908–e2917. doi:10.1093/cid/ciaa1418.

Ong, S.W.X., Tan, Y.K., Chia, P.Y., Lee, T.H., Ng, O.T., Wong, M.S.Y., Marimuthu, K., 2020. Air, Surface Environmental, and Personal Protective Equipment Contamination by Severe Acute Respiratory Syndrome Coronavirus 2 (SARS-CoV-2) From a Symptomatic Patient. JAMA 323, 1610. doi:10.1001/jama.2020.3227.

Paulo, A.C., Correia-Neves, M., Domingos, T., Murta, A.G., Pedrosa, J., 2010. Influenza infectious dose may explain the high mortality of the second and third wave of 1918 1919 influenza pandemic. PLoS ONE 5. doi:10.1371/JOURNAL.PONE.0011655.

Ryan, K.A., Bewley, K.R., Fotheringham, S.A., Slack, G.S., Brown, P., Hall, Y., Wand, N.I., Marriott, A.C., Cavell, B.E., Tree, J.A., Allen, L., Aram, M.J., Bean, T.J., Brunt, E., Buttigieg, K.R., Carter, D.P., Cobb, R., Coombes, N.S., Findlay-Wilson, S.J., Godwin, K.J., Gooch, K.E., Gouriet, J., Halkerston, R., Harris, D.J., Hender, T.H., Humphries, H.E., Hunter, L., Ho, C.M.K., Kennard, C.L., Leung, S., Longet, S., Ngabo, D., Osman, K.L., Paterson, J., Penn, E.J., Pullan, S.T., Rayner, E., Skinner, O., Steeds, K., Taylor, I., Tipton, T., Thomas, S., Turner, C., Watson, R.J., Wiblin, N.R., Charlton, S., Hallis, B., Hiscox, J.A., Funnell, S., Dennis, M.J., Whittaker, C.J., Catton, M.G., Druce, J., Salguero, F.J., Carroll, M.W., 2021. Dose-dependent response to infection with SARS-CoV-2 in the ferret model and evidence of protective immunity. Nature Communications 12, 81. doi:10.1038/s41467-020-20439-y.

Smieszek, T., Lazzari, G., Salathé, M., 2019. Assessing the Dynamics and Control of Droplet- and Aerosol-Transmitted Influenza Using an Indoor Positioning System. Scientific Reports 9, 2185. doi:10.1038/s41598-019-38825-y.

Smith, DH, Gravelle, 2001. The practice of discounting in economic evaluations of healthcare interventions URL: https://eprints.whiterose.ac.uk/.

Stilianakis, N.I., Drossinos, Y., 2010. Dynamics of infectious disease transmission by inhalable respiratory droplets. Journal of The Royal Society Interface 7, 1355–1366. doi:10.1098/rsif.2010.0026.

Tang, S., Mao, Y., Jones, R.M., Tan, Q., Ji, J.S., Li, N., Shen, J., Lv, Y., Pan, L., Ding, P., Wang, X., Wang, Y., MacIntyre, C.R., Shi, X., 2020. Aerosol transmission of SARS-CoV-2? Evidence, prevention and control. Environment International 144, 106039. doi:10.1016/j.envint.2020.106039.

Tellier, R., 2009. Aerosol transmission of influenza A virus: a review of new studies. Journal of The Royal Society Interface 6. doi:10.1098/rsif.2009.0302.focus.

Tellier, R., 2022. COVID-19: the case for aerosol transmission. Interface Focus 12. doi:10.1098/rsfs.2021.0072.

Thorrington, D., van Leeuwen, E., Ramsay, M., Pebody, R., Baguelin, M., 2019. Assessing optimal use of the standard dose adjuvanted trivalent seasonal influenza vaccine in the elderly. Vaccine 37, 2051–2056. URL: https://linkinghub.elsevier.com/retrieve/pii/S0264410X19302932, doi:10.1016/j.vaccine.2019.03.002.

Tokars, J.I., Olsen, S.J., Reed, C., 2018. Seasonal Incidence of Symptomatic Influenza in the United States. Clinical Infectious Diseases 66, 1511–1518. doi:10.1093/cid/cix1060.

Trunfio, M., Calcagno, A., Bonora, S., Di Perri, G., 2021. Lowering SARS-CoV-2 viral load might affect transmission but not disease severity in secondary cases. The Lancet Infectious Diseases 21, 914–915. doi:10.1016/S1473-3099(21)00205-X.

UK Health Security Agency, 2022. COVID-19: epidemiology, virology and clinical features. URL: https://www.gov.uk/government/publications/wuhan-novel-coronavirus-background-information.

Van Damme, W., Dahake, R., van de Pas, R., Vanham, G., Assefa, Y., 2021. COVID-19: Does the infectious inoculum dose-response relationship contribute to understanding heterogeneity in disease severity and transmission dynamics? Medical Hypotheses 146, 110431. doi:10.1016/J.MEHY.2020.110431.

Wardlaw, T.M., Johansson, E.W., Hodge, M.J., 2006. Pneumonia: the forgotten killer of children. UNICEF .

Watson, J.M., Francis, J.N., Mesens, S., Faiman, G.A., Makin, J., Patriarca, P., Treanor, J.J., Georges, B., Bunce, C.J., 2015. Characterisation of a wild-type influenza (A/H1N1) virus strain as an experimental challenge agent in humans. Virology Journal 12. URL: /pmc/articles/PMC4322439//pmc/articles/PMC4322439/?report=abstracthttps://www.ncbi.nlm.nih.gov/pmc/articles/PMC4322439/, doi:10.1186/S12985-015-0240-5.

Weinstein, R.A., Bridges, C.B., Kuehnert, M.J., Hall, C.B., 2003. Transmission of Influenza: Implications for Control in Health Care Settings. Clinical Infectious Diseases 37, 1094–1101. doi:10.1086/378292.

World Health Organisation, 2018. Seasonal Influenza Factsheet. URL: https://www.who.int/news-room/fact-sheets/detail/influenza-(seasonal).

World Health Organisation, 2022a. Coronavirus (COVID-19) Dashboard URL: https://covid19.who.int/.

World Health Organisation, 2022b. International Guidelines for Certification and Classification (Coding) of COVID-19 as Cause of Death. URL: https://www.who.int/publications/m/item/international-guidelines-for-certification-and-classification-(coding)-of-covid-19-as-cause-of-death.

World Health Organization, 2022. Plague. URL: https://www.who.int/news-room/fact-sheets/detail/plague.

Wu, J., Zha, P., Med, C., 2020. Association of COVID-19 Disease Severity with Transmission Routes and Suggested Changes to Community Guidelines URL: www.igoosa.com., doi:10.20944/preprints202003.0246.v1.

Zala, D., Mosweu, I., Critchlow, S., Romeo, R., McCrone, P., 2020. Costing the COVID-19 Pandemic: An Exploratory Economic Evaluation of Hypothetical Suppression Policy in the United Kingdom. Value in Health 23, 1432–1437. doi:10.1016/j.jval.2020.07.001.

Supplementary Information

S1. Background: The biological evidence for a symptom severity mapping

To motivate the development of a mathematical model with mechanisms that can capture the propagation of symptom severity (described in Section 2), I initially expand on the contemporary biological knowledge for the existence of a symptom severity mapping. This will consist of an exploration of the mechanisms of the transmission of respiratory pathogens and the pathways through which a symptom severity mapping could exist, and then a summary of the evidence available for three respiratory diseases: Plague, influenza and COVID-19.

Pathways for the propagation of symptom severity

While limited observational data is available to quantify a symptom severity mapping for respiratory diseases, emerging evidence supports pathways through which it could occur. These two pathways, which will be discussed in detail in the following subsections, are through a dose-response relationship and differential transmission routes.

Dose-response relationship

The dose-response relationship is the relationship between an individual's infectious dose and their subsequent disease severity and transmissibility. There is strong evidence across the literature that viral shedding, measured by the number of viral particles detected, is positively correlated with symptom severity in the case of influenza (Couch et al., 1971; Bjornson et al., 1991; Hall et al., 1979), SARS (Chu et al., 2004) and MERS (Al-Abdely et al., 2019). This correlation means that individuals with more severe disease are likely to infect others with a higher infectious dose than if they had milder disease. Suppose a dose-response relationship exists for a particular respiratory pathogen. In that case, we expect this higher infectious dose to lead to more severe disease in those infected, resulting in a symptom severity mapping.

The existence of a dose-response relationship seems to vary across respiratory infections. In some cases, there seems to be strong evidence in favour of its existence as seen with measles (Aaby and Coovadia, 1985) and certain respiratory bacteria (Jones and Su, 2015). However, for others, there is limited evidence and the existence of a dose-response relationship is still up for debate.

Differential transmission routes

The other motivating factor for a symptom severity mapping involves the transmission route. There are three predominant routes of transmission for most respiratory pathogens: contact (either direct or indirect), large droplet and aerosol transmission (Killingley and Nguyen-Van-Tam, 2013). Contact transmission is where viral particles are "picked up" on hands either through direct contact with an infected individual or from contact with a contaminated surface. These particles are then transferred to the respiratory tract via contact with the face and deposit in the upper respiratory tract (URT). Large droplet transmission involves particles larger than 10μm, which are generally released through coughs and sneezes. These particles can travel up to a metre through the air and deposit in the URT. Due to the similarity of transmission properties of these two routes (i.e. both act over short distances and deposit in the URT), they are often considered together as close contact transmission (CCT). Aerosol transmission involves particles smaller than 5μm, which are generally released through coughs and normal breathing. They are sufficiently light to travel on air flows and potentially allow for longer distance transmission. These particles can be inhaled and primarily deposit in the lower respiratory tract (LRT), although they may also deposit in the URT (Tellier, 2009).

Since severe disease is often indicated by the development of a cough, we expect that its subsequent transmission will be to some extent driven by aerosol transmission, as opposed to predominately being driven by CCT. There is strong evidence across respiratory infections that infection via aerosol transmission causes more severe disease than

that caused by CCT. This is thought to be because aerosol transmission leads to particles mainly depositing in the LRT (Tellier, 2009), which is likely to result in reactivity of the airway and cause a cough, leading to severe disease.

Whilst the impact of the transmission route on symptom severity in the infectee is well established, the relative importance of the different transmission routes is debated (Hall et al., 1979) and the impact of the symptom severity of the infector on the transmission route is unclear. We assume mild disease spreads predominantly through CCT and severe disease spreads through aerosol transmission and CCT, though further research is required. It may be that either CCT or aerosol transmission is dominant in both cases, leading to symptom severity having a limited impact on the transmission route and, therefore, the subsequent symptom severity of those infected.

Evidence for specific diseases

Whether or not a symptom severity mapping exists, and the extent to which it exists, is likely to vary between respiratory diseases; this is exemplified by the three diseases considered in detail here (plague, influenza, COVID-19).

Plague

One respiratory disease with clear evidence of a symptom severity mapping is plague, caused by the bacterium *Yersinia pestis*. Plague predominantly comes in one of two forms: bubonic and pneumonic (Dean et al., 2018). Bubonic plague is typically transmitted between humans by ectoparasites such as fleas or lice (Drancourt et al., 2006) and can develop into pneumonic plague if the bacteria enter and infect the lungs (Gani and Leach, 2004). Pneumonic plague is a more severe form of plague (Centers for Disease Control and Prevention, 2021) with a mortality rate close to 100% when left untreated (World Health Organization, 2022). Individuals with pneumonic plague can then infect others via aerosol transmission (Gani and Leach, 2004). Individuals infected via this route are infected with pneumonic plague, unlike transmission through all other routes which result in bubonic plague. The existence of a symptom severity mapping for plague suggests the potential for a symptom severity mapping for other respiratory diseases, especially if the aerosol route of transmission is involved.

Influenza

It is currently unclear whether such a symptom severity mapping exists for influenza as there is still widespread debate over its transmission mechanisms.

There is limited evidence for influenza that a dose-response relationship exists. Some studies found that a higher inoculant dose leads to more severe symptoms (Han et al., 2019) whereas others found that severe disease had no association with the dose given (Watson et al., 2015). One review even found that across 55 experimental studies there was no correlation between the inoculant dose and the prevalence of cough and a negative correlation between the dose and the prevalence of fever (Carrat et al., 2008).

A symptom severity mapping through differential transmission routes does seem to have more substantial support. There is evidence that intranasal inoculation causes a significantly smaller proportion of cases to be severe (Carrat et al., 2008) when compared to natural infections (Cao et al., 2009; Moser et al., 1979; Little et al., 1979). Intranasal inoculation leads to infection mainly in the URT, similar to infection from CCT. Intranasal inoculation leading to a smaller proportion of severe cases could be explained by natural infection being driven by aerosol transmission which leads to more severe disease. This hypothesis is supported by animal model studies of influenza using ferrets which found a clear relationship between the transmission route and the resulting disease (Herlocher et al., 2001; Bodewes et al., 2011) with intranasal inoculation generally leading to mild disease with infection predominately in the URT and aerosol inoculation causing infection in the LRT leading to more severe disease.

However, the relative importance of the different transmission routes is debated (Hall et al., 1979). Whilst some argue that droplets drive influenza transmission (Aledort et al., 2007; Weinstein et al., 2003; Brankston et al., 2007) others argue that droplet transmission would be a rare event (Atkinson and Wein, 2008; Killingley and Nguyen-Van-Tam, 2013). Similarly, there is uncertainty about the importance of the aerosol transmission route (Smieszek et al., 2019). Many argue that aerosol transmission is unlikely due to a lack of evidence of long-range transmission (Awofeso et al., 2001; Apisarnthanarak and Mundy, 2010; Moser et al., 1979). Yet, others argue that is contributes majorly to the spread of influenza Cowling et al. (2013) and some suggest aerosol transmission dominates in certain scenarios (Atkinson and Wein, 2008; Stilianakis and Drossinos, 2010; Killingley and Nguyen-Van-Tam, 2013).

COVID-19

Whilst a symptom severity mapping for COVID-19 is not confirmed, emerging evidence supports its existence.

The impact of viral load on disease severity of COVID-19 in humans is debated (Van Damme et al., 2021; Trunfio et al., 2021). However, evidence for a dose-response relationship is emerging in animal-model studies. These studies found that higher initial viral inoculum was associated with increased viral shedding and more severe disease (Imai et al., 2020; Ryan et al., 2021).

The debate over the relative importance of different transmission routes has been reignited in the context of COVID-19. Some believe that transmission of *SARS-CoV-2* is mainly through respiratory droplets and contact with infected surfaces rather than through aerosols (Karimzadeh et al., 2021), mainly due to a lack of evidence for long-distance transmission (Ong et al., 2020). However, there is strong support for the importance of the aerosol transmission route (Tellier, 2022; Lelieveld et al., 2020; Tang et al., 2020; Morawska and Cao, 2020), leading many to believe that it is the primary transmission route.

Additionally, there is evidence that aerosol transmission leads to more severe disease (Tellier, 2022) suggesting the possibility of a symptom severity mapping through differential transmission routes for COVID-19.

S2: Calculating the final size of the epidemic

With the addition of multiple infectious classes, calculating the final size becomes much more complicated. Instead, we can consider a simplified SEIR model with no symptom severity classes (**??**) from which we can predict the final size of the outbreak given a value of R_0.

$$\begin{aligned}
\frac{dS}{dt} &= -\frac{\beta S I}{N} \\
\frac{dE}{dt} &= \frac{\beta S I}{N} - \epsilon E \\
\frac{dI}{dt} &= \epsilon E - \gamma I \\
\frac{dR}{dt} &= \gamma I
\end{aligned}$$

We want to calculate the final size of the epidemic, which is given by $R(\infty)$. Since there is no demography or waning immunity to replenish the susceptible class, $I \to 0$, $E \to 0$ and $R \to R_\infty$ as $t \to \infty$. Thus $S \to N - R_\infty$. To find R_∞ we have to find R in terms of S which can be done by dividing $\frac{dS}{dt}$ by $\frac{dR}{dt}$:

$$\frac{dS}{dR} = -\frac{\beta}{\gamma}\frac{S}{N} = -R_0\frac{S}{N}$$

We can solve this to get:

$$S(t) = S(0)e^{-\frac{R_0}{N}\left(R(t)-R(0)\right)}$$

So taking $t \to \infty$,

$$S_\infty = N - R_\infty = S(0)e^{-\frac{R_0 R_\infty}{N}}$$

i.e.

$$R_\infty = N - S(0)e^{-\frac{R_0 R_\infty}{N}}$$

Solving this equation is equivalent to finding the fixed point of $f(x) = N - S(0)e^{-\frac{R_0 x}{N}}$, i.e. a point such that $f(x) = x$. This can be done through fixed point iteration which is where $x_{n+1} = f(x_n)$. This fixed point then gives a value of R_∞ for a set value of R_0.

S3. Infection-blocking intervention model

In this section I have described a model that includes an intervention with an infection-blocking effect, in addition to reducing the likelihood of having severe disease. Those who are protected have mild disease with probability η if they would have otherwise had severe disease and are not infected with probability η if they would have had mild disease (Fig. S1).

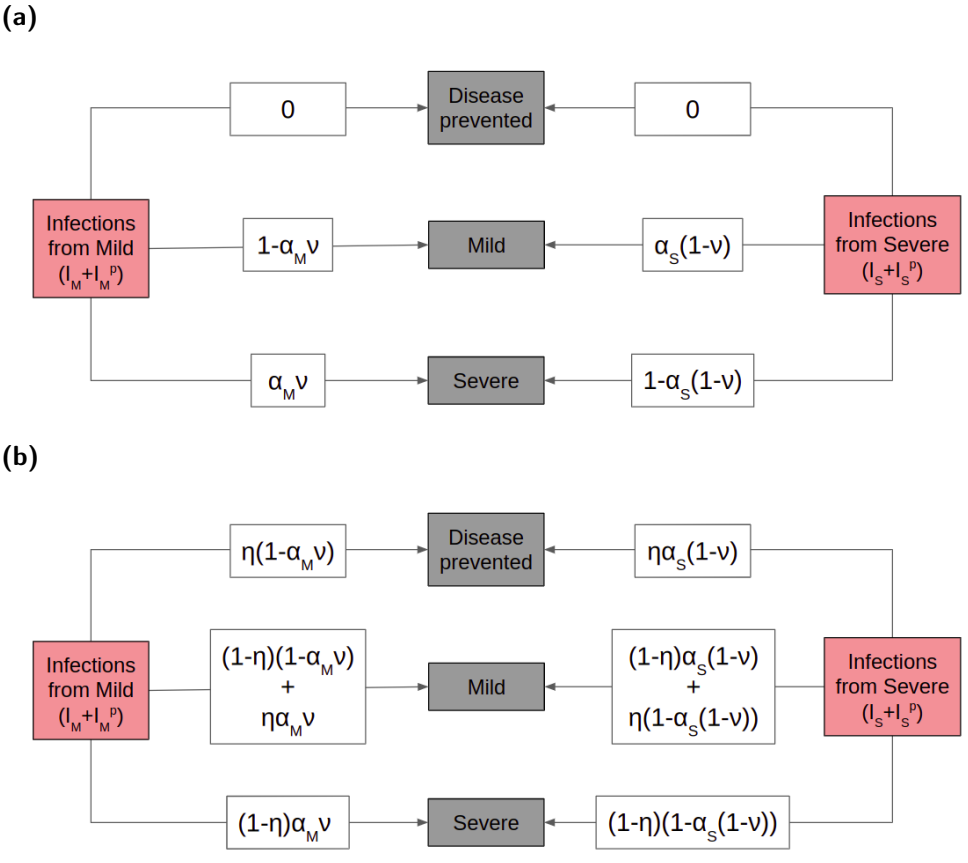

Figure S1: The proportion of cases with each symptom severity level resulting from infections by individuals with symptom severity s. I present two scenarios: (a) no intervention is used and (b) the infection-blocking intervention is used.

The equations below govern the model which includes the intervention. Here the p notation (as in S^p) indicates that the individuals in that class are protected by the intervention.

$$\frac{dS}{dt} = -(\lambda_M + \lambda_S)S$$

$$\begin{aligned}\frac{dE_M}{dt} &= (1-\alpha_M\nu)\lambda_M S + \alpha_S(1-\nu)\lambda_S S \\ &\quad - \epsilon E_M\end{aligned}$$

$$\begin{aligned}\frac{dE_S}{dt} &= \alpha_M\nu\lambda_M S + (1-\alpha_S(1-\nu))\lambda_S S \\ &\quad - \epsilon E_S\end{aligned}$$

$$\frac{dI_M}{dt} = \epsilon E_M - \gamma_M I_M$$

$$\frac{dI_S}{dt} = \epsilon E_S - \gamma_S I_S$$

$$\frac{dR_M}{dt} = \gamma_M I_M$$

$$\frac{dR_S}{dt} = \gamma_S I_S$$

$$\begin{aligned}\frac{dS^p}{dt} &= -(1-\eta(1-\alpha_M\nu))\lambda_M S^p \\ &\quad - (1-\eta\alpha_S(1-\nu))\lambda_S S^p\end{aligned}$$

$$\begin{aligned}\frac{dE_M^p}{dt} &= \eta(\alpha_M\nu\lambda_M + (1-\alpha_S(1-\nu))\lambda_S)S^p \\ &\quad + (1-\eta)((1-\alpha_M\nu)\lambda_M + \alpha_S(1-\nu)\lambda_S)S^p \\ &\quad - \epsilon E_M^p\end{aligned}$$

$$\begin{aligned}\frac{dE_S^p}{dt} &= (1-\eta)(\alpha_M\nu\lambda_M + (1-\alpha_S(1-\nu))\lambda_S)S^p \\ &\quad - \epsilon E_M^p\end{aligned}$$

$$\frac{dI_M^p}{dt} = \epsilon E_M^p - \gamma_M I_M^p$$

$$\frac{dI_S^p}{dt} = \epsilon E_S^p - \gamma_S I_S^p$$

$$\frac{dR_M^p}{dt} = \gamma_M I_M^p$$

$$\frac{dR_S^p}{dt} = \gamma_S I_S^p$$

$$\lambda_M = \frac{\beta_M(I_M + I_M^p)}{N}$$

$$\lambda_S = \frac{\beta_S(I_S + I_S^p)}{N}$$

S4. Deriving an equation for R_0

In the two symptom severity case I was able to write down an equation for R_0 since it is an eigenvalue of $\mathbf{K}$ and thus solves

$$\begin{aligned}0 &= \lambda^2 - (k_{MM} + k_{SS})\lambda + (k_{MM}k_{SS} - k_{MS}k_{SM}) \\ &= \lambda^2 - \left(\frac{\beta_M}{\gamma_M}(1-(1-\alpha_M)\nu) + \frac{\beta_S}{\gamma_S}(1-(1-\alpha_S)(1-\nu))\right)\lambda + \frac{\beta_M\beta_S}{\gamma_M\gamma_S}(1-(1-\alpha_M)\nu - (1-\alpha_S)(1-\nu)) \\ &= \lambda^2 - \left(\frac{\beta_M}{\gamma_M}(1-(1-\alpha_M)\nu) + \frac{\beta_S}{\gamma_S}(1-(1-\alpha_S)(1-\nu))\right)\lambda + \frac{\beta_M\beta_S}{\gamma_M\gamma_S}(\alpha_M\nu + \alpha_S(1-\nu))\end{aligned} \tag{4}$$

i.e

$$\begin{aligned}2\lambda_\pm &= \left(\frac{\beta_M}{\gamma_M}(1-(1-\alpha_M)\nu) + \frac{\beta_S}{\gamma_S}(1-(1-\alpha_S)(1-\nu))\right) \\ &\quad \pm \sqrt{\left(\frac{\beta_M}{\gamma_M}(1-(1-\alpha_M)\nu) + \frac{\beta_S}{\gamma_S}(1-(1-\alpha_S)(1-\nu))\right)^2 - 4\frac{\beta_M\beta_S}{\gamma_M\gamma_S}(\alpha_M\nu + \alpha_S(1-\nu))}\end{aligned}$$

R_0 is the dominant eigenvalue of $\mathbf{K}$, i.e. the eigenvalue with the largest absolute value. Since $\beta, \gamma > 0$ and $\alpha, \nu \in [0,1]$, $\left(\frac{\beta_M}{\gamma_M}(1-(1-\alpha_M)\nu) + \frac{\beta_S}{\gamma_S}(1-(1-\alpha_S)(1-\nu))\right) > 0$, so $R_0 = \lambda_+$ i.e.

$$2R_0 = \left(\frac{\beta_M}{\gamma_M}(1-(1-\alpha_M)\nu) + \frac{\beta_S}{\gamma_S}(1-(1-\alpha_S)(1-\nu))\right) + \sqrt{\left(\frac{\beta_M}{\gamma_M}(1-(1-\alpha_M)\nu) + \frac{\beta_S}{\gamma_S}(1-(1-\alpha_S)(1-\nu))\right)^2 - 4\frac{\beta_M\beta_S}{\gamma_M\gamma_S}(\alpha_M\nu + \alpha_S(1-\nu))} \tag{5}$$

S5. Explanation of α causing a reduction in total infections

When the infectious period of severe disease, $T_S = \frac{1}{\gamma_S}$ is longer than that of mild disease, T_M, the proportion of cases that are severe increases. When a higher proportion of cases are severe, we expect that a symptom severity mapping would amplify this effect. So, when $T_S > T_M$, the proportion of cases that are severe, and therefore the value of R_0, is expected to substantially increase for $\alpha > 0$ compared to when $\alpha = 0$. So to maintain the fixed value of R_0, β has to be reduced more for $\alpha > 0$.

However, in reality, the increase in severe cases is mostly seen in the long-term dynamics near the end of the outbreak (Fig. S2, top row). The proportion of cases that are severe at the start of the outbreak increases relatively minimally with T_S when α is close to 0. This means that the increase in α has less of an amplifying affect than expected since by the time the proportion of severe cases increases significantly, relatively few individuals are being infected. So the overall proportion of cases that are severe has increased by less than expected when $\alpha > 0$, meaning that β has been set to be lower than required. As α increases further towards 1, the effect of $T_S > T_M$ reduces since now the majority of cases are severe even at the start of the outbreak.

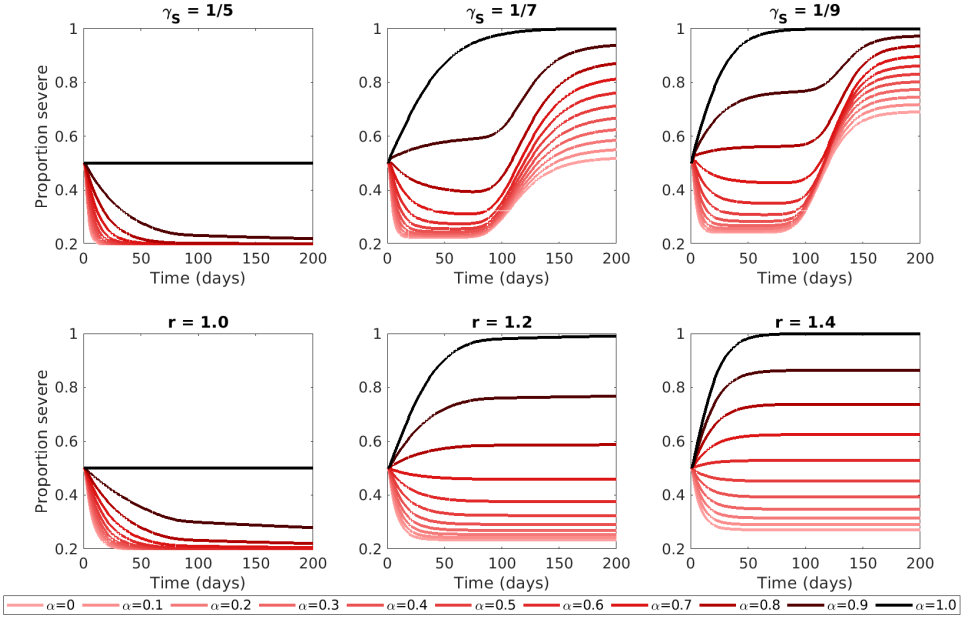

Figure S2: Investigating how the proportion of cases that are severe changes over time. In these plots, the proportion of cases that are severe refers to the proportion of currently infectious individuals that are severe. The first row is when $\beta_S = \beta_M$ and $\gamma_S \geq \gamma_M = 1/5$. The second row is when $\beta_S \geq \beta_M$ and $\gamma_S = \gamma_M$. All other parameters are as in Table 1 and R_0 is set to 3.0. The shading of the lines corresponds to the value of α with darker lines corresponding to a stronger symptom severity mapping.

When the transmission rate was instead increased, I found that the proportion of cases that were severe increased as well (Fig. S2, bottom row). However, this increase occurred from the start of the outbreak meaning that when $\alpha > 0$ the effect was amplified. Hence, there is no substantial reduction in the number of infections when the severe transmission rate is increased.

S6. Additional figures

This section contains additional figures which are referenced throughout the results (Section 3).

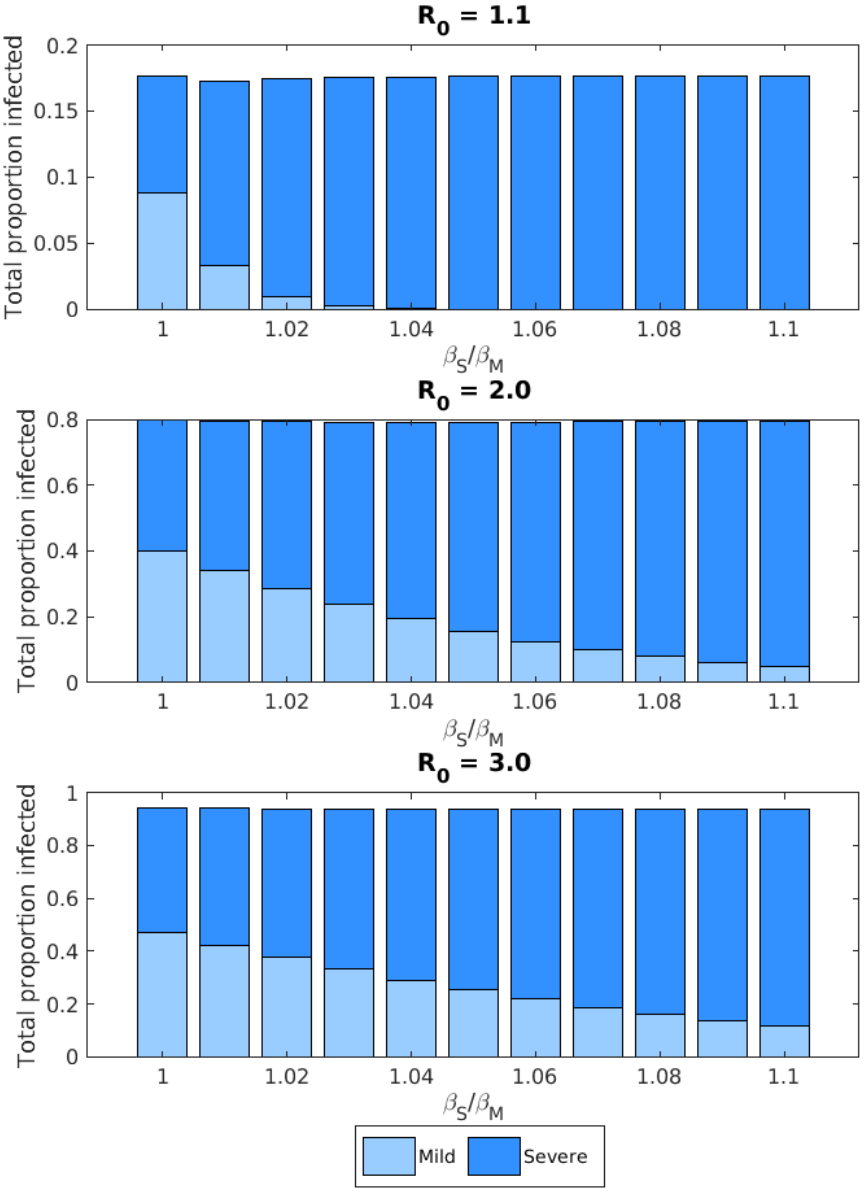

Figure S3: Exploring the effect of increasing the severe transmission rate when $\alpha = 1$. Recall that $\alpha = 1$ corresponds to symptom severity always passing on with infection. In this scenario, mild and severe disease have equal infectious durations and the baseline probability of severe disease is $\nu = 0.5$.

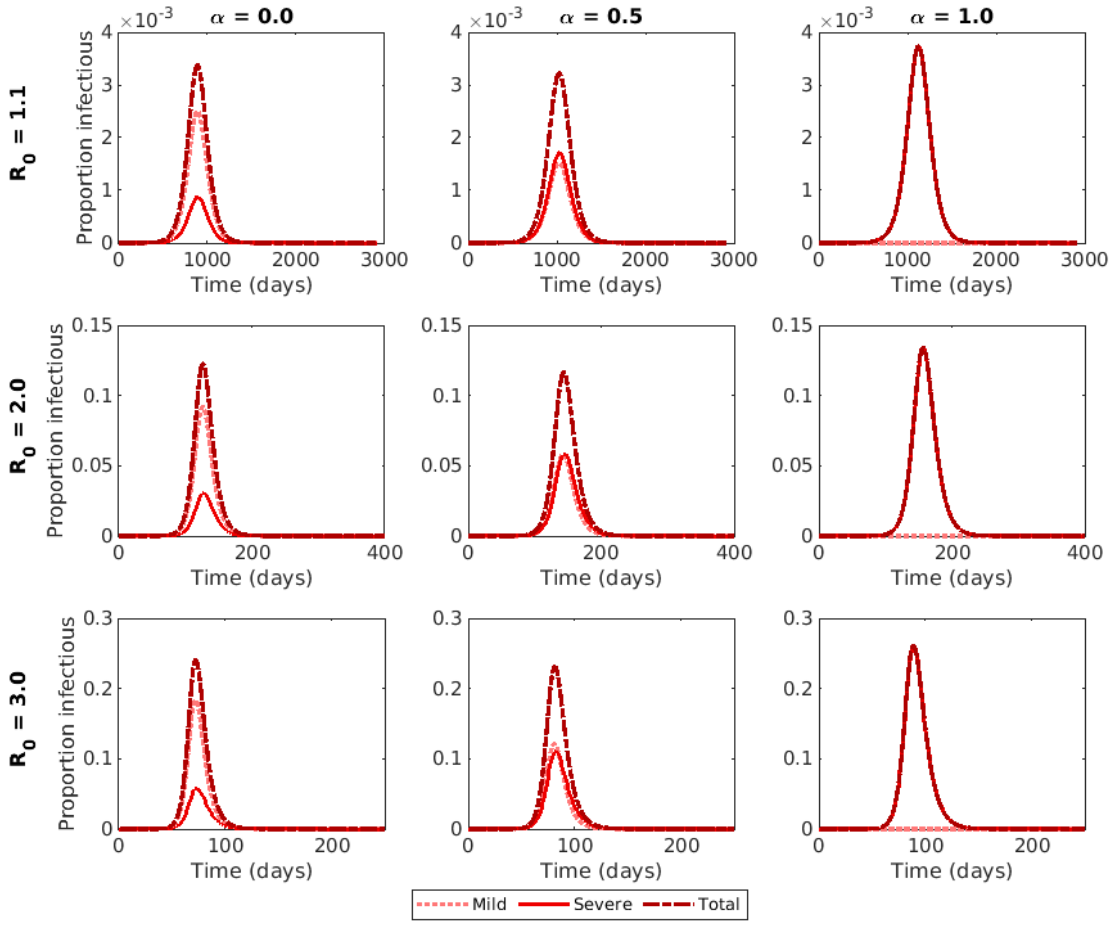

Figure S4: Temporal plots of the outbreak across three values of R_0 and three values of α. The parameters used are as described in Table 1. The line style and shading denotes the severity of the infected class. The dotted line shows the proportion of the population in the mild infectious class, the solid line shows the proportion of the population in the severe infectious class and the dashed line shows the total proportion of the population infectious.

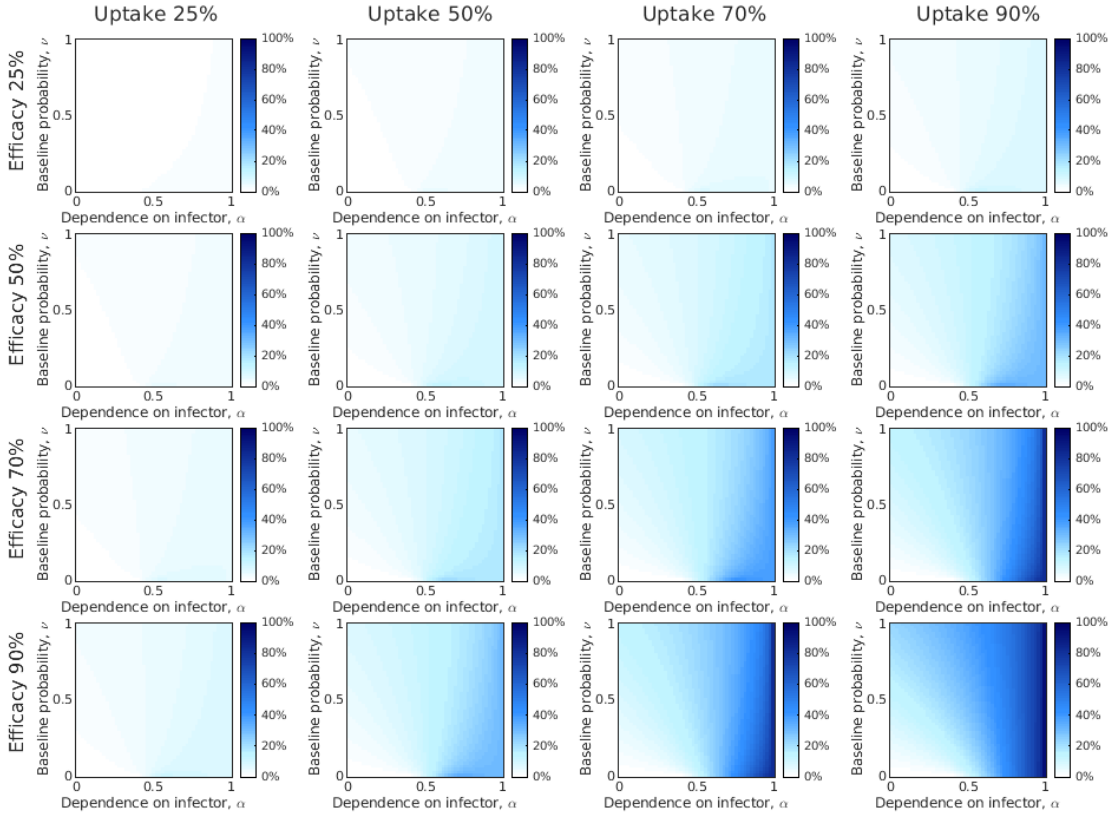

Figure S5: Investigating the percentage of infections prevented by the intervention. For each uptake and efficacy and values of ν and α, the total number of infections at the end of the simulation are subtracted from the total number of infections in the no intervention scenario for those values of ν and α to give the number of infections prevented. The darker shading corresponds to a larger percentage of infections being prevented.

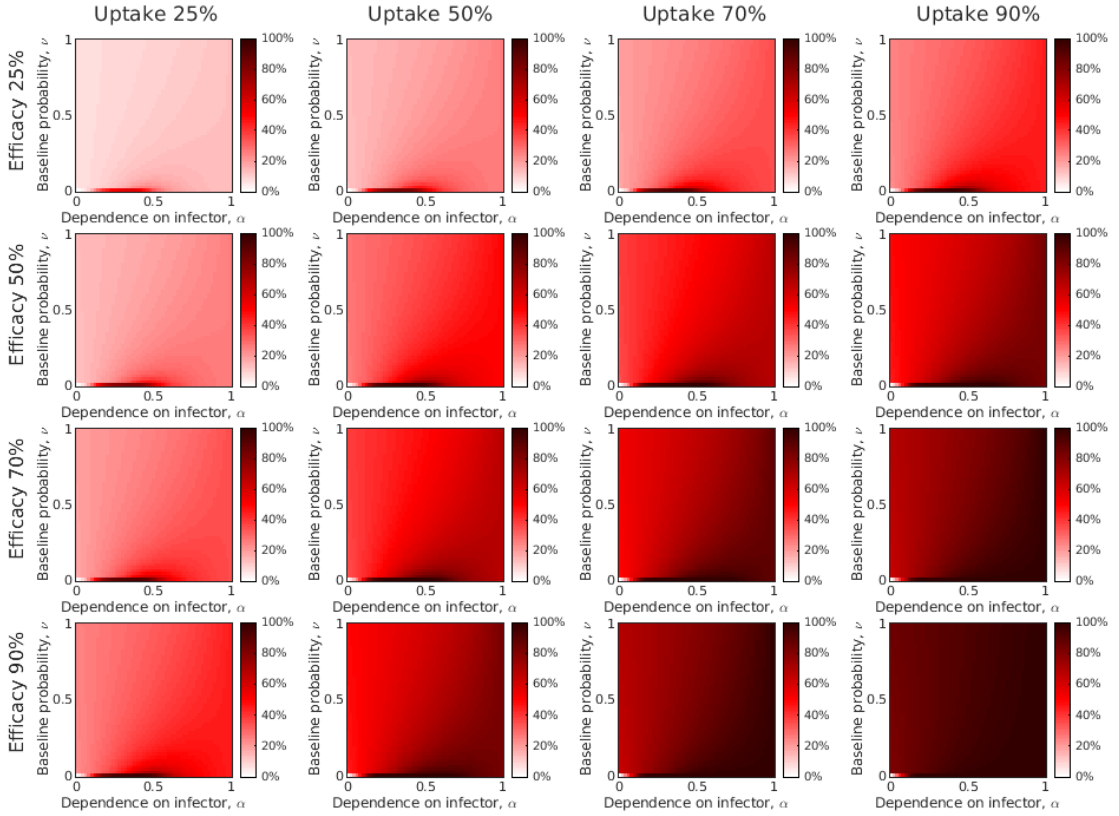

Figure S6: Investigating the percentage of severe infections prevented by the intervention. For each uptake and efficacy and values of ν and α, the total number of severe infections at the end of the simulation are subtracted from the total number of severe infections in the no intervention scenario for those values of ν and α to give the number of severe infections prevented. The darker shading corresponds to a larger percentage of severe infections being prevented.

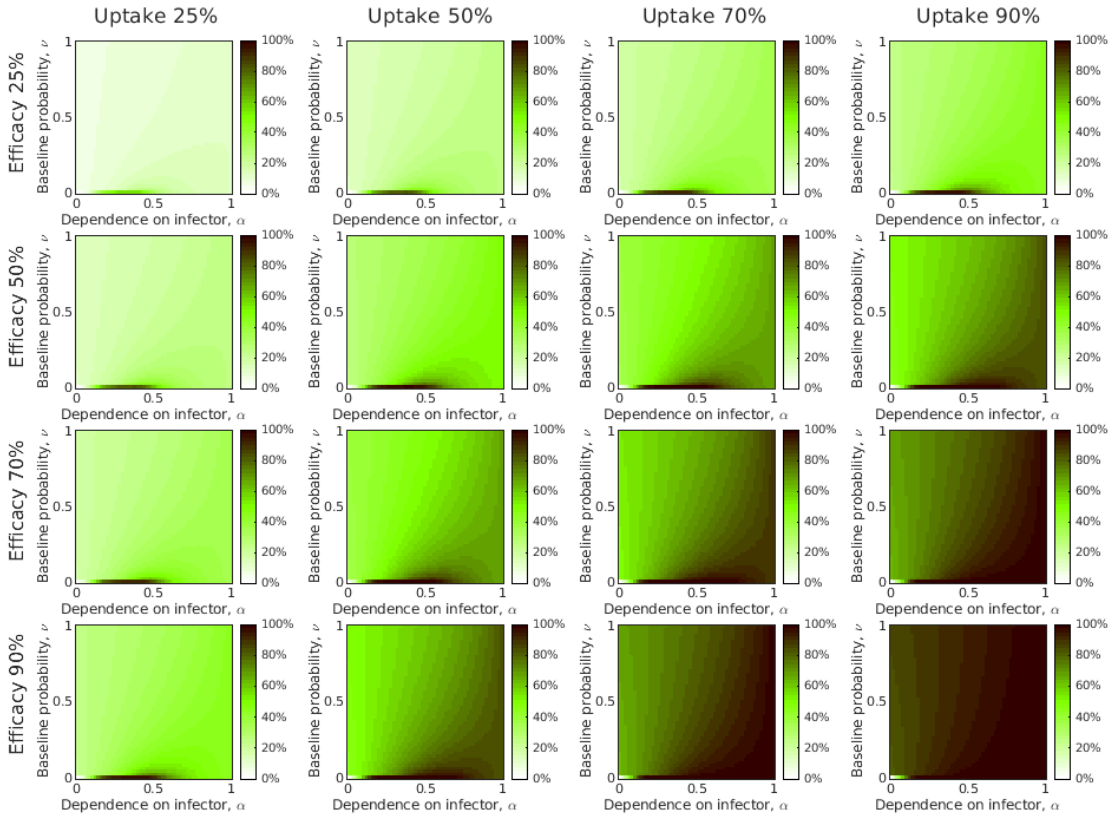

Figure S7: Investigating the percentage of hospitalisations prevented by the intervention. For each uptake and efficacy and values of ν and α, the total number of hospitalisations at the end of the simulation are subtracted from the total number of hospitalisations in the no intervention scenario for those values of ν and α to give the number of hospitalisations prevented. The darker shading corresponds to a larger percentage of hospitalisation being prevented.